Title: Multiomics analyses decipher intricate changes in the cellular and metabolic landscape of steatotic livers upon dietary restriction and sleeve gastrectomy

Authors: Shuai Chen[1#], Qinghe Zeng[2,3#], Xiurong Cai[4,5], Jiaming Xue[1], Peng Song[1], Liming Tang[1], Christophe Klein[3], Frank Tacke[6], Adrien Guillot[6*], Hanyang Liu[1,6*]

Affiliations:
[1]Department of General Surgery, The Affiliated Changzhou Second People's Hospital of Nanjing Medical University, Changzhou Medical Center, Nanjing Medical University, Changzhou 213000, China.
[2]Laboratoire d'Informatique Paris Descartes (LIPADE), Université Paris Cité, Paris 75014, France.
[3]Centre d'Histologie, d'Imagerie et de Cytométrie (CHIC), Centre de Recherche des Cordeliers, INSERM, Sorbonne Université, Université de Paris, Paris 75014, France.
[4]The Jackson Laboratory, Bar Harbor, ME, USA.
[5]Department of Hematology, Oncology and Tumor Immunology, Charité Universitätsmedizin Berlin, Campus Virchow-Klinikum, Berlin 13353, Germany.
[6]Department of Hepatology and Gastroenterology, Charité Universitätsmedizin Berlin, Campus Virchow-Klinikum and Campus Charité Mitte, Berlin 13353, Germany.

*Corresponding author.
1. Hanyang Liu, Department of Hepatology and Gastroenterology, Charité Universitätsmedizin Berlin, Campus Virchow-Klinikum and Campus Charité Mitte, 13353 Berlin, Germany.
Email: hanyang.liu@charite.de
2. Adrien Guillot, Department of Hepatology and Gastroenterology, Charité Universitätsmedizin Berlin, Campus Virchow-Klinikum and Campus Charité Mitte, 13353 Berlin, Germany.
Email: adrien.guillot@charite.de

# These authors contributed equally.

One Sentence Summary: Multiomics analyses demonstrate dynamic cellular crosstalk therapeutic mechanisms in steatotic livers upon dietary restriction and sleeve gastrectomy.

Abstract: Metabolic dysfunction-associated steatotic liver disease (MASLD) is a chronic, progressive liver disease that encompasses a spectrum of steatosis, steatohepatitis (or MASH), and fibrosis. Evidence suggests that dietary restriction (DR) and sleeve gastrectomy (SG) can lead to remission of hepatic steatosis and inflammation through weight loss, but it is unclear whether these procedures induce distinct metabolic or immunological changes in MASLD livers. This study aims to elucidate the intricate hepatic changes following DR, SG or sham surgery in rats fed a high-fat diet as a model of obesity-related MASLD, in comparison to a clinical cohort of patients undergoing SG. Single-cell and single-nuclei transcriptome analysis, spatial

metabolomics, and immunohistochemistry revealed the liver landscape, while circulating biomarkers were measured in serum samples. Artificial intelligence-assisted image analysis characterized the spatial distribution of hepatocytes, myeloid cells and lymphocytes. In patients and experimental MASLD rats, SG improved BMI, circulating liver injury biomarkers and triglyceride levels. Both DR and SG attenuated liver steatosis and fibrosis in rats. Metabolism-related genes (*Ppara*, *Cyp2e1* and *Cyp7a1*) were upregulated in hepatocytes upon DR and SG, while SG broadly upregulated lipid metabolism on cholangiocytes, monocytes, macrophages, and neutrophils. Furthermore, SG promoted myeloid cell accumulation in the liver not only ameliorating inflammation but activating liver repair processes. Regions with potent myeloid infiltration were marked with enhanced metabolic capacities upon SG. Additionally, a disruption of periportal hepatocyte functions was observed upon DR. In conclusion, this study indicates a dynamic cellular crosstalk in steatotic livers undergoing SG. Notably, PPARα- and gut-liver axis-related processes, and metabolically-active myeloid cell infiltration indicate intervention-related mechanisms supporting SG for the treatment of MASLD.

Keywords: MASLD; NAFLD; Weight loss; Bariatric surgery; Liver macrophage; Immunometabolism; Liver zonation; Deep learning; Gut-liver axis

Main Text:

INTRODUCTION

Obesity and overweight represent significant global health challenges, affecting approximately 2 billion people worldwide (1). Obesity-related complications encompass a spectrum of metabolic syndromes, including metabolic dysfunction-associated liver diseases (MASLD), metabolic dysfunction-associated steatohepatitis (MASH) and multi-organ disorders, contributing to elevated mortality rates among affected individuals (2, 3). MASLD encompasses a range of chronic liver pathologies affecting more than a quarter of the global population, characterized predominantly by steatosis and fibrosis, with potential progression to cirrhosis and hepatocellular carcinoma and potent immune cell involvement at all disease stages (4). Despite considerable research efforts, pharmacotherapeutic targets for MASLD remain largely elusive, with only a limited number of candidates demonstrating efficacy. Only recently, resmetirom (a selective thyroid hormone receptor beta agonist) was approved by the Food and Drug Administration (FDA), USA as the first treatment of patients with MASH with moderate to advanced liver fibrosis, along with diet management and exercise (5).

Lifestyle modifications, such as dietary restriction (DR) and exercise, remain the mainstay of recommended therapeutic interventions in overweight and obese individuals with MASLD, with the aim of reducing body weight by at least 10% (6). However, the sustainability of long-term (hypocaloric) dietary management poses several challenges, particularly for individuals with severe obesity (7). Consequently, bariatric surgery (BS) has emerged as a viable option for obese patients, particularly when conventional nutritional and behavioral therapy fails to achieve desired therapeutic outcomes. In a randomized controlled clinical trial, BS-based interventions were superior to lifestyle intervention alone in weight loss as well as in improving histological features of MASLD such as resolution of MASH and improvement of liver fibrosis by at least 1 stage (8). Furthermore, observational studies demonstrated long-term benefits regarding cardiovascular and liver-related morbidity as well as mortality (9).

Among various surgical modalities, sleeve gastrectomy (SG) is the most frequently performed procedure, supported by robust evidence of long-term efficacy and safety (10). SG restricts nutritional intake by reducing the stomach volume and capacity, without reconstructing the gastrointestinal tract (11). Emerging studies have suggested that BS potentially mitigates lipid accumulation and halts MASLD progression (12-14). Furthermore, Although the primary consequence of SG is the restriction of food intake, akin to dietary restriction (DR) without surgery, SG induces favorable alterations in systemic inflammation and gut microbiota composition (15). Recent advancements in omics technologies allow for sophisticated inquiries into liver diseases from diverse angles, including gene expression, protein function, metabolism, and microbiome activity, which paved the way for dissecting hepatic alterations upon weight-loss management with an unprecedented resolution (16). Our previous research demonstrated that BS exerts superior protective effects in livers from patients with MASLD compared to DR, a finding associated with increased macrophage infiltration in BS (13).

Here, we sought to compare the molecular and cellular consequences of DR and SG related to the ameliorated of liver steatosis, using a rodent obesity-MASLD model. Single-cell (sc)/single-nuclei (sn) transcriptome analysis was utilized to describe intracellular alterations and extracellular interactions, while spatial metabolomics with the assistance of artificial intelligence (AI)-based image analysis was implemented to decipher metabolite production collating immune cell zonation. We provide novel insights into multiomics alterations in steatotic livers undergoing DR and SG, which may hopefully facilitate understanding mechanistic consequences of surgery-based therapies in MASLD.

RESULTS

SG induces weight loss and ameliorates non-invasive biomarkers in human patients with MASLD

BMI and serological indexes were analyzed retrospectively in 18 patients who underwent SG (Figure 1A). In comparison to baseline at one day pre-SG, significant declines of BMI, postprandial blood glucose (PPG), aspartate aminotransferase (AST), alanine aminotransferase (ALT), gamma-glutamyltransferase (γ-GT), triglycerides (TG), high-density lipoprotein-cholesterol (HDL-C) and TBIL occurred at 6 months post-SG, while total bile acids (TBA) ($p = 0.051$) and fibroblast growth factor (FGF)-19 ($p = 0.058$) tended to increase (Figure 1B-D, Table S1). This data hence revealed profound changes in varying processes, including inflammatory, metabolic and gut-derived endocrine signals. Intriguingly, male patients benefitted more from SG particularly on serological TG and low-density lipoprotein-cholesterol (LDL-C) levels than female patients (Table S2). Thus, and to further investigate the cellular mechanisms involved in the liver response to SG and compare with DR, healthy wild-type male rats were used to recapitulate interventions on an obesity-related MASLD model (Figure 2A, Figure S1). All rats gained weight after 12 weeks of a high-fat diet (HFD) feeding, whereas Sham + DR and SG had a reduced weight gain in the 8 weeks following the intervention compared to HFD alone. Moreover, SG was the most efficient approach to halt weight gain (Figure 2B). Serum analysis revealed that in comparison to Sham animals on HFD, Sham + DR rats had lower levels of LDL. SG significantly suppressed levels of TG, LDL and AST, but increased the levels of HDL, TBA and FGF-19. Additionally, SG drastically suppressed cholesterol levels ($p = 0.06$) but led to increased serum FGF-21 ($p = 0.06$) (Figure 2C). HFD exaggerated hepatic lipid accumulation in

comparison to rats fed a normal diet. Yet, both Sham + DR and SG intervention dramatically diminished hepatic lipid accumulation compared to the HFD-fed sham group (Figure 2D and E). Simultaneously, fibrosis was increased after HFD, while it was significantly attenuated by both DR and SG (Figure 2F and G). Results imply that both DR and SG effectively ameliorated obesity, liver steatosis and fibrosis, while SG was the most efficient intervention for improving systemic levels of lipid metabolism and bile acid (BA) production.

Sc/sn-transcriptome analysis evidences an altered hepatic cellular landscape after DR and SG

Rat liver samples (n=3 each per Sham [on HFD], Sham + DR and SG group) were analyzed using sc/snRNA-sequencing analysis, with an explicit classification of main hepatic and immune cell populations [including hepatocytes, cholangiocytes, hepatic stellate cells (HSC), endothelial cells, macrophages, monocytes, neutrophils, dendritic cells (DC), B cells, T cells and NK cells] (Figure 3A, Figure S2A and B). Reconstituted cell composition suggested higher numbers of NK cells, B cells, neutrophils and cholangiocytes leading to a lower proportion of hepatocytes and hepatic stellate cells upon Sham + DR (vs. Sham). In contrast, SG intervention led to increased proportions of macrophages and cholangiocytes but fewer monocytes and DCs (Figure 3A). Metabolism-related marker expression (*Cyp2e1*, *Cyp7a1*, *Ppara*, *Nr1h4*, *Pnpla3* and *Gcg*) in liver steatosis was detected in hepatocytes and immune cells, and these pathways were transcriptionally regulated in Sham + DR and SG groups (*vs.* Sham) (Figure 3B). IHC evidenced that PNPLA3 protein was significantly downregulated in Sham + DR and SG groups (*vs.* Sham), while PPARα-expressing liver cells increased in the SG group (*vs.* Sham) (Figure 3C and D), thereby confirming the profound regulation towards beneficial metabolic pathways in hepatocytes on a protein level after SG.

Furthermore, differentially expressed genes (DEGs) were screened in parenchymal (Figure 4A) and immune cells (Figure 4B) by comparing Sham + DR and SG to Sham groups. Transcriptomic influences of diverse cell types in the liver upon Sham + DR and SG were assessed based on cell proportions and significant DEG numbers. The distance of dots to value '0' can be considered as magnitude of influences. Data shows that hepatocytes and cholangiocytes were most influenced by SG, indicating a substantial impact of SG on metabolic functions of liver parenchymal cells, whereas endothelial cells were most influenced by Sham + DR (Figure 4C), indicating ameliorated endothelial dysfunction as a consequence of DR. In accordance with the Kyoto Encyclopedia of Genes and Genomes (KEGG) database, enriched signaling pathways were identified based on significantly upregulated DEGs. Up- and down-regulated DEGs at the bulk levels were compared between Sham, Sham + DR and SG groups, indicating enhanced metabolic processes (SG *vs.* Sham and SG *vs.* Sham + DR) and declined metabolic processes (Sham + DR *vs.* Sham) (Figure S3B), which were in line with findings on liver samples from patients from our earlier study (13).

Next, regulated signaling pathways were compared between the groups (Sham + DR *vs.* Sham, SG *vs.* Sham, and SG *vs.* Sham + DR) for each cell population (Figure 5A). Fatty acid degradation-related gene expression was increased not only in hepatocytes (Sham + DR *vs.* Sham, SG *vs.* Sham, SG *vs.* Sham + DR) but also in cholangiocytes and endothelial cells (SG *vs.* Sham). Furthermore, PPAR signaling pathways, fatty acid degradation and cholesterol metabolism were more pronounced (not only in hepatocytes) by both Sham + DR and SG interventions (*vs.* Sham). Interestingly, in comparison to Sham + DR, the PPAR signaling pathway was promoted in cholangiocytes, endothelial cells and myeloid cell populations

(monocytes, macrophages, DCs and neutrophils). Of note, butanoate metabolism was enhanced in hepatocytes upon both Sham + DR and SG (Figure 5A). In addition, cellular interactions (total and ligand-receptor) were elucidated between each gradual pair of cell types among all three groups using the CellChat algorithm (Figure S4A and B). Key signaling pathways that enriched according to total cellular interactions were described (Figure S5A). In contrast to Sham, both Sham + DR and SG elevated ligand reception of neutrophils from immune cells, while SG elevated ligand release from cholangiocytes to other cells. Of note, in contrast to Sham + DR groups, SG promoted interaction levels of non-hepatocyte parenchymal cells (cholangiocytes, HSCs and endothelial cells) as well as immune cells (mainly for macrophages and neutrophils) (Figure 5B). Further dissecting cholangiocyte-associated cellular interactions, significant signaling pathways from cholangiocytes to monocytes, macrophages, neutrophils, B lymphocytes, T lymphocytes and NK cells, as well as from monocytes, macrophages, DCs, hepatocytes, T lymphocytes and NK cells to cholangiocytes were illustrated (Figure S5B and C).

Taken together, both Sham + DR and SG improve liver lipid metabolism (remarkably PPAR-associated processes) in steatotic livers. In particular, SG triggers metabolic enhancement broadly in liver cells, including hepatocytes, cholangiocytes, endothelial cells and myeloid cells. Additionally, cholangiocytes appear to actively interact with multiple liver cell types upon SG.

SG promotes liver metabolic capacities by accumulating myeloid cell population

To explore the metabolic landscape of the liver, three representative liver samples were freshly acquired from the Sham, Sham + DR and SG groups and then analyzed using an ambient MSI metabolomics approach (Figure 6A). The spectrum and distribution of total metabolites (with positive and negative ions) were illustrated (Figure S6A – E). Histological features of liver samples together with spatially distributed metabolite abundance were displayed, indicating strongly reduced production of total metabolites in steatotic livers undergoing DR or SG (Figure 6B). Function enrichment analysis based on the total abundance of differentially upregulated metabolites illustrated that both Sham + DR and SG enhanced lipid metabolism in steatotic livers in contrast to Sham groups, potentially attenuating steatotic stress in the liver. It is worth noting that SG significantly enhanced the capacities of linoleic acid metabolism, fat digestion and absorption, and cholesterol metabolism compared to Sham + DR (Figure 6C).

Artificial intelligence (AI)-based pathological exploration has evolved as a promising and precise tool for MASLD investigations (17). Hence in this study, a deep-learning model was established based on cell annotations (hepatocytes, lymphocytes and myeloid cells) that were supervised by liver pathology experts (Figure 7A). Accordingly, numbers of hepatocytes, lymphocytes and myeloid cells were assessed on a total of 18 rat liver samples. Importantly, hepatocyte proportions (70 – 80%) of total liver cells were not significantly altered by different interventions (Figure 7B). Lymphocyte proportions were significantly increased in Sham with HFD (1.5 – 6.1%) *vs.* healthy control (0.05 -2.1%) but declined upon Sham + DR (0.7 – 2.0%) and SG (0.5 – 2.2%) (*vs.* Sham) (Figure 7B). Simultaneously, SG exacerbated the infiltration of myeloid cells (*vs.* healthy control, *vs.* Sham + DR) (Figure 7B). In comparison, the numbers of lymphocytes and myeloid cells were assessed based on the sc/sn RNA-seq dataset. Myeloid cell proportions tended to increase by SG (Figure S7A and B). Besides, the cell distribution of lymphocytes and myeloid cells was depicted to correspondingly map the metabolites in diverse cell regions (Figure 7C). The abundance of total metabolites between regions with high or low myeloid cell infiltration was compared (high-/low-infiltration region selection displayed in Figure 7C). SG remarkably increased metabolite abundance in regions with high myeloid cell

221 infiltration (Figure 7D). In addition, upregulated metabolites in regions rich in myeloid cells
222 significantly refer to processes of autophagy, together with the metabolism of choline, linoleic
223 acids, cholesterol and glycerophospholipids (Figure 7E). Given the diverse phenotypic functions
224 of macrophages in the liver, a list of markers (*Trem2*, *Spp1*, *Gpnmb*, *Mmp9*, *Mmp13*, *Plin2*,
225 *Ppara*, *Pparg*, *Cd207*, *Cx3cr1*, *Clec4f*, *Nos2*, *Cd80*, *Nlrp3*, *Il1b*, *Tnfa*, *Cd163*, *Mrc1*, *Il10* and
226 *Tgfb1*) was selected from the sc/sn RNA-seq dataset to assess phenotypes of scar-associated
227 macrophage (SAM), lipid-associated macrophage (LAM), liver capsular macrophage (LCM),
228 Kupffer cell (KC), pro- and anti-inflammatory macrophages (18-20). Comparing macrophage
229 clusters (SG vs. Sham), markers of SAM, LCM and KC were upregulated (SG *vs.* Sham),
230 whereas pro-inflammatory macrophage markers were downregulated (SG *vs.* Sham and Sham +
231 DR *vs.* Sham) (Figure 7F, Figure S7C). Simultaneously, SG promoted classical phenotypes of
232 monocytes bur suppressed neutrophil maturation. In contrast, DR tended to promote
233 conventional DC phenotype and neutrophil maturation (Figure 7F, Figure S7C). Taken together,
234 SG and DR enhanced lipid metabolism in the liver, while SG promoted myeloid cell
235 accumulation in the liver, facilitating metabolic improvement and liver repair processes.

236 **SG facilitates liver repair processes in steatotic livers**

237 The strong accumulation of macrophages in SG-treated livers, in conjunction with the weight
238 development and metabolic improvement, suggested the induction of myeloid cell-driven hepatic
239 repair processes (21). To further assess the cellular phenotypic alterations in the liver, a list of
240 markers was explored (for hepatocytes: *Pcna*, *Ppara*, *Cyp2e1*, *Cyp7a1* and *Afp*; for
241 cholangiocytes: *Pcna*, *Sox9*, *Slc4a2*, *Hnf4a* and *Hnf1b*; for HSCs: *Pdgfrb*, *Tgfb1*, *Col1a1*, *Acta2*
242 and *Vim*) (Figure 8A). The expression of *Pcna*, *Ppara*, *Cyp2e1* and *Cyp7a1* in hepatocytes, the
243 expression of *Pcna* and *Hnf1b* in cholangiocytes, and the expression of *Pdgfrb* in HSCs were
244 significantly upregulated by SG (*vs.* Sham). In contrast, the expression of *Pcna* in hepatocytes
245 and cholangiocytes, together with the expression of *Pdgfrb* were downregulated by Sham + DR
246 (*vs.* Sham) (Figure 8A). Besides, cell differentiation was assessed and depicted using a cell
247 trajectory analysis model (Figure 8B). Cell trajectory of hepatocytes implied higher expression
248 of *Pcna*, *Cyp2e1* and *Ppara* in Sham + DR and SG groups than the Sham group, while the
249 expression distinctly varied with the cell trajectory (Figure 8B, Figure S3C). Cholangiocytes
250 were classified into three groups. Cholangiocytes from Sham and SG groups were more
251 associated with the expression of *Pcna* and *Slc4a2* but not with the expression of *Sox9* (Figure
252 8B, Figure S3C). Furthermore, HSCs of Sham + DR groups were shown in relatively inactivated
253 clusters with low *Pdgfrb* expression (Figure 8B), but not correlated with the expression of Tgfb1
254 and Col1a1 (Figure S3B). In addition, CK7-expressing cells accumulated more in Sham and SG
255 groups (*vs.* Ctrl and *vs.* Sham + DR) (Figure 8C and D). Simultaneously, interleukin (IL)-17A-
256 expressing cells increased in Sham groups (*vs.* Ctrl) but decreased in Sham + DR and SG groups
257 (*vs.* Sham) (Figure 8C and D). Taken together, SG can facilitate liver repair processes by
258 enhancing the proliferation of hepatocytes and cholangiocytes, as well as fueling the fibrogenesis
259 of HSCs.

260 **DR affects zonation characteristics of periportal hepatocytes**

261 Given the remarkable cell trajectory with variable expression of phenotypic markers, differential
262 characteristic alterations in hepatocyte subtypes were hypothesized. Hence, hepatocytes were
263 further dissected into subpopulations based on sc/sn RNA-seq dataset (Figure 9A). Metabolism-
264 related function enrichment analysis revealed two distinct groups: metabolism one group (Met1,
265 including cluster 6, 7 and 10) enriched metabolism processes of glycolysis, lipids and drugs,

while metabolism two groups (Met2, including clusters 1, 2, 3, 4, 5, 8 and 9) enriched fatty acid biosynthesis (Figure 9B). Interestingly, illustrations of the gene expression (pericentral hepatocyte markers: *Ctnnb1*, *Cnne1*, *Lrp5*, *Lrp6*, *Myc* and *Glul*; periportal hepatocyte markers: *Cyp2f2* and *Alb*) further identified that the Met1 group harbors more periportal hepatocytes, while the Met2 group harbors more pericentral hepatocytes (Figure 9C and D). Furthermore, cell trajectory analysis indicated the explicit differentiation status of these two metabolism groups, which supports the zonal classification (Figure 9E). In comparison to periportal (Met1) hepatocytes, pericentral (Met2) hepatocytes illustrated higher numbers and strength of interactions with immune cells, while myeloid cells, T lymphocytes and NK cells exerted particularly high involvement in cellular interactions (Figure S8A and B). Particularly, periportal hepatocytes accounted for 15 - 20% of total hepatocytes in both Sham and SG groups but were almost absent (0.4%) in the Sham + DR group (Figure 9F). Strikingly, proliferative cells ($Ki67^{+}$) were more present in the liver tissues of Sham and SG groups in comparison to Ctrl groups. Significantly, SG enhanced cell proliferation among all groups (Figure 9G). In addition, metabolism markers (CYP2E1 and CYP7A1) and cell proliferation (Ki67) were investigated in situ. CYP2E1 and CYP7A1 were determined to be more enriched surrounding central veins in Ctrl, Sham and SG groups, but to be homogeneously distributed in Sham + DR groups (Figure 9G and H). In addition, the spatial metabolite distribution of fatty acids, BAs and sphingolipids appeared to be enriched around periportal areas in Sham and SG groups but rather widely spread in Sham + DR groups (Figure 9I). Taken together, DR reshapes hepatocyte zonation features potentially by depriving periportal hepatocyte characteristics, which may compromise the capacities of metabolism and regeneration in steatotic livers in comparison to SG.

DISCUSSION

In this study, we employed multiomics methods to elucidate significant attenuation of obesity-related parameters and liver steatosis following SG and DR in both patient cohorts and rat models. Specifically, sc/sn RNA-seq data unveiled an augmentation of lipid metabolism in both hepatocytes and immune cells, with a notable emphasis on myeloid cells following SG. Furthermore, spatial metabolomics analysis revealed the strengthened metabolic capacities of liver cells induced by SG and DR. Notably, SG elicited elevated lipid metabolic capacities in regions exhibiting heightened myeloid cell infiltration, underscoring the intricate interplay between metabolic and immune responses in the liver microenvironment. PPAR-α emerged as a prominent factor mediating the observed metabolic enhancements induced by both SG and DR. Additionally, the increased serological levels of bile acids and gut-derived FGF-19, together with hepatic butanoate metabolism underscored the pivotal roles of the gut-liver axis in modulating liver metabolism post-SG.

To date, only a few studies employing the bulk-RNA transcriptome analysis of patients' liver samples post-BS to identify transcriptome alterations of inflammation and lipid metabolism, suggesting potential therapeutic mechanisms of MASLD (22). Essentially, PPARα was elucidated as a key nuclear receptor that regulates weight-loss-induced MASLD amelioration (23, 24). The PPAR agonism has been regarded as a promising approach to improving MASLD (25, 26). Robust preclinical data have determined the potential of targeting PPARα to improve lipid metabolism, inflammation, and fibrosis in MASLD (27, 28). Our previous study has proved that the elevating PPAR levels by lanifibranor (a pan-PPAR agonist) significantly improves liver steatosis and fibrosis in in-vivo mouse and in-vitro liver-on-a-chip models of MASLD (29).

However, numerous PPAR dual/pan agonists have failed to reach the endpoint, because of diverse side-effect events (e.g., liver injury, worsened fibrosis, increasing liver fat volumes) (30).

Noteworthy, immunometabolism enhancement, especially on myeloid cell populations, was revealed in post-SG steatotic livers. Myeloid cells, especially macrophages, play a pivotal role in pathological and therapeutic mechanisms of metabolic liver diseases (26, 31, 32). The involvement of liver macrophages can mediate hepatic lipid metabolism during steatotic stress (33, 34), while lipid metabolism is closely associated with phenotypic alterations in macrophages (35, 36). Thus, the liver macrophage remains a novel target for MASLD therapies (37-39). In addition, SG effectively enhanced the PPARα level and metabolic pathways broadly on hepatic parenchymal and immune cells, superior to DR. It has been demonstrated that PPARα activation in the liver can ameliorate the accumulation of circulating monocytes upon DR intervention (40). Intriguingly, in rat MASLD models, SG can strengthen the macrophage pool despite a broad PPARα activation in the liver. Further characterization of the macrophage population indicates that SG endows the anti-inflammatory and repair-associated potential of macrophages rather than promotes inflammation in the liver.

Given the essential roles of gut-derived signals in the liver, the current understanding of MASLD pathogenesis lacks insights into gut-liver crosstalk, encompassing hepatic cell metabolism, inflammation, fibrogenesis, and complex cellular interactions, which likely play pivotal roles in MASLD progression (21, 26, 41). Increasing evidence indicates critical roles that BS may play in regulating the gut-liver axis, including GM, and BA metabolism (42). As suggested by recent studies, post-BS changes in the GM and BA circulation, as well as a decrease in the portal influx of free fatty acids, are beneficial to steatotic livers (43, 44). BAs regulate the composition of microbial communities and the outcome of surgical obesity in terms of body weight (45). As characterized, BAs revive insulin sensitivity and reduce gluconeogenesis, enhancing glucose metabolism (46). Furthermore, BS can drastically repopulate GM and reverse the primary/secondary BA ratio in the intraluminal ileal, inducing improvement in metabolic syndrome in patients with MASLD (47). Similarly, our study determined improved capacities of BA secretion and butanoate metabolism, as well as elevated FGF19 levels in serum upon the SG, suggesting that SG influences liver metabolism by regulating the gut-liver axis. On the other hand, the butanoate production by GM was reported to be associated with bile acids and mediating liver metabolism (48). Notably, butanoate production can be enhanced after bariatric surgery (49).

To note, our single-cell and spatial analysis characterized hepatocyte zonation features by a list of common zonation markers and metabolic activity profiling, indicating potential regulatory roles during DR and SG interventions. The hepatocyte functional zonation has been characterized by differences in metabolism, xenobiotic processing and repair capacities (50). Emerging studies demonstrated that absent metabolic function in the periportal zone provokes cholestasis and ductular reaction (51). On the other hand, compromised hepatic periportal characteristics may be attributed to the dysregulated WNT signaling and cell regeneration, which fuels the potential hepatic carcinogenesis (51, 52). In this study, hepatic periportal characteristics were dramatically subsided by DR, whereas preserved by SG. Since DR is rarely associated with adverse events in the liver, we hypothesize that periportal hepatocytes might temporarily acquire ‘pericentral’ features to support hepatic metabolism. In contrast, enhanced immunometabolism levels may interpret the preservation of zonal features upon the SG intervention. However, the mechanisms remain unclear yet.

Essentially, the limitations inherent in the current study should be acknowledged. Firstly, the sample size utilized for spatial metabolomics analysis was relatively modest, potentially constraining the generalizability of the findings. Secondly, the absence of a mapped spatially resolved transcriptomic analysis may have hindered the characterization of additional cell populations necessary for metabolite detection at a single-cell level. Additionally, the exclusion of patients with MASLD and obesity who solely underwent DR for disease modification constitutes a limitation. This exclusion stemmed from challenges associated with dietary normalization to SG and inherent biases in dietary quantification. Furthermore, it remains challenging to distinguish the precise causes of liver steatosis improvement between weight-loss and surgical interference.

MATERIALS AND METHODS

Human cohort

The clinical retrospective study was conducted on 18 patients who received SG in Changzhou Second People's Hospital (from January 2023 to July 2023). This cohort comprised n=8 male (44.4%) and n=10 female (55.6%) individuals at a median age of 34 years (range: 29 - 40). We included patients that fulfilled the following criteria: 1) BMI > 32.5 kg/m2; 2) Age: 16 – 65; 3) clinically diagnosed with MASLD (based on cardiometabolic risk factors and presence of steatosis on liver imaging; 4) diagnosed with type 2 diabetes or sleep apnea syndrome; 5) without a history of other hepatic or genetic illness; 6) received sleeve gastrectomy, without postoperative complications. Clinical indexes (e.g., BMI, serological indexes) were evaluated on the day before SG and 6 months post-surgery. This clinical retrospective study was approved by the ethics committee of the Affiliated Changzhou No. 2 People's Hospital of Nanjing Medical University (ID: [2023]KY124-01).

Animal models and surgical interventions

Male wild-type SPRAGUE DAWLEY® rats aged 8 weeks were obtained from Laboratory Animal Co., Ltd. (Changzhou, China). Rats were bred under specific-pathogen-free conditions and fed an HFD (D12492, Research Diets, Inc., USA) for 12 weeks. Five rats received sham surgery followed by uncontrolled HFD, 9 rats received sleeve gastrectomy followed by uncontrolled HFD, and 8 rats received sham surgery followed by restricted HFD feeding (comparable to dietary intake of post-SG rats) for 8 weeks. Procedures of sleeve gastrectomy were illustrated in supplementary data (Supplementary Methods and Figure S1) and were based on our previous research (53). Five healthy control rats were set with normal diet feeding but without any specific interventions. All these procedures were performed and supported by Kerbio Co., Ltd., Changzhou, China. Animal experiments were approved by the Institutional Animal Care and Use Committee (ID: IACUC23-0068).

Serological tests

Patients' blood samples were acquired from the median cubital vein. Rat blood samples were harvested through rat hearts immediately after rats were sacrificed. Serum was harvested using centrifugation (450×g, 10 min), and stored at -80℃. Circulating markers including AST, ALT, PPG, γ-GT, TG, cholesterol (CHO), HDL-C, LDL-C, alkaline phosphatase (ALP) and TBA were measured using Indiko analyzer (ThermoFisher, USA). Cytokines including IL-6, IL-10, FGF-19, FGF-21 and transferrin (TRF) were measured using ELISA kits and a microplate reader

399 (Rayto, China). All measurements were conducted following the manufacturer's instructions.
400 Antibodies that were used in this study are listed in Table S2.

401 **Immunohistochemistry and tissue staining**

402 Liver tissues were harvested immediately after rats were sacrificed. Tissues were fixed in 10%-
403 formalin for 24 hours, followed by paraffin embedding. Sections of 5 μm thickness were
404 obtained using a HistoCore BIOCUT microtome (Leica, Germany). Hematoxylin and eosin
405 (H&E) staining were performed using standard procedures. Extracellular collagen area was
406 indicated using the Picro Sirius Red Stain Kit (Abcam, UK). Immunohistochemistry (IHC) was
407 employed using the kits purchased from Beyotime Biotechnology, China. Antigen retrieval was
408 conducted using a heat-induced epitope retrieval method within a citrate buffer. Primary
409 antibodies against the target proteins were applied, followed by appropriate secondary
410 antibodies. Diaminobenzidine (DAB) was used for chromogenic detection, and counterstaining
411 was performed with hematoxylin. Slides were examined under a microscope to evaluate protein
412 localization and expression levels. In situ staining was observed under a light microscope
413 (Olympus, Japan). Antibodies used in this study are listed in Table S2. For the quantitation of
414 cell nucleus and protein levels, FIJI software was utilized (54). In particular, relative staining
415 densities of proteins per μm^2 were assessed and compared between peri-central and -portal
416 regions in each tissue slide.

417 **Single-cell and single-nuclei sequencing and analysis**

418 Single cells and cell nuclei were isolated and extracted from freshly collected rat liver samples
419 using the dissection kit purchased from OE Biotech Co., Ltd., Shanghai, China. The libraries
420 were acquired following the manufacturer's protocol and then sequenced using the MobiNova
421 platform (Shanghai, China). The integration of sc/sn-RNA sequencing data was operated
422 following the common protocol with eliminating batch effects (55). Cell Ranger was used to
423 filter the data, while the downstream analyses were conducted using Seurat (V5.0.1) (56),
424 CellChat (1.6.0) (57), and Monocle2 (58) software packages for R. Function enrichment was
425 performed based on KEGG databases. All the technical procedures including sampling, quality
426 control, library build-up and sequencing analysis were supported by the genome platform of OE
427 Biotech Co., Ltd., Shanghai, China.

428 **Spatial metabolomics analysis**

429 Liver samples were freshly acquired from rats and then frozen at -80°C immediately after
430 optimal cutting temperature (OCT) embedding. Embedded tissue samples were sliced into 5 μm
431 using a cryo-microtome CM 1950 (Leica, Germany). In-situ profiles of total metabolites were
432 detected with positive and negative ion binding approaches using the mass spectrometry imaging
433 (MSI) metabolomics method (59). Tissue regions were annotated after H&E staining. Metabolite
434 enrichment was assessed based on the KEGG database. All the technical procedures including
435 sample preparation, quality control, detection and analysis were supported by the metabolomics
436 platform of Luming Biotechnology Co., Ltd. Shanghai, China.

437 **AI-guided imaging analysis**

438 The AI-guided imaging analysis performed herein is based on a previously published approach
439 (60-62). H&E-stained rat liver sections were scanned using a light microscope (Olympus, Japan).
440 Processing of the whole slide images (WSIs) was operated using QuPath 0.4.4 following a pre-
441 defined protocol (63). Sparse annotations, comprising approximately 15 cells for each of the cell

442 populations, were manually labeled across three WSIs representing different conditions (Sham,
443 Sham + DR and SG). A simple artificial neural network classifier with two hidden layers,
444 consisting of 20 and 10 neurons, respectively, was trained to distinguish between the three
445 classes versus the rest. Example regions without these classes were used as negative examples
446 during training. Subsequently, cell classification and measurements were exported, and for each
447 cell population, 2D hexagonal binning plots of the number of cells were generated in Python
448 (using the matplotlib function 'hexbin') (64). The model was trained for representative cells (at
449 least 15 cells / sample' of hepatocytes, lymphocyte-like cells and myeloid-like cells) based on
450 three liver tissue slides, which were defined with the assistance of pathological expertise. The
451 trained model was applied to the sample cohort of rat liver sections (including 5 Ctrl, 5 Sham, 8
452 Sham + DR and 8 SG samples). Detailed methodology is described in the Supplementary
453 methods.

454 **Statistical analysis**

455 The GraphPad Prism 9.0 software (GraphPad Software, USA) and the ggplot2 package (version:
456 3.4.4) for R were used to generate plots (65). The statistical tests used in this study are indicated
457 in the figure legend for each panel. Data are presented as the mean ± S.D. '$p < 0.05$' was
458 considered a significant difference.

459

460 **List of Supplementary Materials**

461 Supplementary methods and figures

462 Table S1. Clinical follow-up data

463 Table S2. List of antibodies used in this study.

464

465 **References and Notes**

466 1. N. C. D. R. F. Collaboration, Worldwide trends in underweight and obesity from 1990 to
467 2022: a pooled analysis of 3663 population-representative studies with 222 million
468 children, adolescents, and adults. Lancet 403, 1027-1050 (2024).

469 2. N. J. Pillon, R. J. F. Loos, S. M. Marshall, J. R. Zierath, Metabolic consequences of
470 obesity and type 2 diabetes: Balancing genes and environment for personalized care. Cell
471 184, 1530-1544 (2021).

472 3. J. Quek, K. E. Chan, Z. Y. Wong, C. Tan, B. Tan, W. H. Lim, D. J. H. Tan, A. S. P.
473 Tang, P. Tay, J. Xiao, J. N. Yong, R. W. Zeng, N. W. S. Chew, B. Nah, A. Kulkarni, M.
474 S. Siddiqui, Y. Y. Dan, V. W. Wong, A. J. Sanyal, M. Noureddin, M. Muthiah, C. H. Ng,
475 Global prevalence of non-alcoholic fatty liver disease and non-alcoholic steatohepatitis in
476 the overweight and obese population: a systematic review and meta-analysis. Lancet
477 Gastroenterol Hepatol 8, 20-30 (2023).

478 4. H. Devarbhavi, S. K. Asrani, J. P. Arab, Y. A. Nartey, E. Pose, P. S. Kamath, Global
479 burden of liver disease: 2023 update. J Hepatol 79, 516-537 (2023).

480 5. S. A. Harrison, P. Bedossa, C. D. Guy, J. M. Schattenberg, R. Loomba, R. Taub, D.
481 Labriola, S. E. Moussa, G. W. Neff, M. E. Rinella, Q. M. Anstee, M. F. Abdelmalek, Z.

482 Younossi, S. J. Baum, S. Francque, M. R. Charlton, P. N. Newsome, N. Lanthier, I.
483 Schiefke, A. Mangia, J. M. Pericas, R. Patil, A. J. Sanyal, M. Noureddin, M. B. Bansal,
484 N. Alkhouri, L. Castera, M. Rudraraju, V. Ratziu, M.-N. Investigators, A Phase 3,
485 Randomized, Controlled Trial of Resmetirom in NASH with Liver Fibrosis. N Engl J
486 Med 390, 497-509 (2024).

487 6. M. E. Rinella, B. A. Neuschwander-Tetri, M. S. Siddiqui, M. F. Abdelmalek, S.
488 Caldwell, D. Barb, D. E. Kleiner, R. Loomba, AASLD Practice Guidance on the clinical
489 assessment and management of nonalcoholic fatty liver disease. Hepatology 77, 1797-
490 1835 (2023).

491 7. F. L. Greenway, Physiological adaptations to weight loss and factors favouring weight
492 regain. Int J Obes (Lond) 39, 1188-1196 (2015).

493 8. O. Verrastro, S. Panunzi, L. Castagneto-Gissey, A. De Gaetano, E. Lembo, E. Capristo,
494 C. Guidone, G. Angelini, F. Pennestri, L. Sessa, F. M. Vecchio, L. Riccardi, M. A.
495 Zocco, I. Boskoski, J. R. Casella-Mariolo, P. Marini, M. Pompili, G. Casella, E. Fiori, F.
496 Rubino, S. R. Bornstein, M. Raffaelli, G. Mingrone, Bariatric-metabolic surgery versus
497 lifestyle intervention plus best medical care in non-alcoholic steatohepatitis (BRAVES): a
498 multicentre, open-label, randomised trial. Lancet 401, 1786-1797 (2023).

499 9. A. Aminian, A. Al-Kurd, R. Wilson, J. Bena, H. Fayazzadeh, T. Singh, V. L. Albaugh, F.
500 U. Shariff, N. A. Rodriguez, J. Jin, S. A. Brethauer, S. Dasarathy, N. Alkhouri, P. R.
501 Schauer, A. J. McCullough, S. E. Nissen, Association of Bariatric Surgery With Major
502 Adverse Liver and Cardiovascular Outcomes in Patients With Biopsy-Proven
503 Nonalcoholic Steatohepatitis. JAMA 326, 2031-2042 (2021).

504 10. L. Zhang, W. H. Tan, R. Chang, J. C. Eagon, Perioperative risk and complications of
505 revisional bariatric surgery compared to primary Roux-en-Y gastric bypass. Surg Endosc
506 29, 1316-1320 (2015).

507 11. B. C. Brajcich, E. S. Hungness, Sleeve Gastrectomy. JAMA 324, 908 (2020).

508 12. A. P. Lopez Lopez, S. Tuli, M. Lauze, I. Becetti, C. C. Pedreira, F. A. Huber, E.
509 Omeroglu, V. Singhal, M. Misra, M. A. Bredella, Changes in Hepatic Fat Content by CT
510 1 Year After Sleeve Gastrectomy in Adolescents and Young Adults With Obesity. J Clin
511 Endocrinol Metab 108, e1489-e1495 (2023).

512 13. S. Chen, L. Tang, A. Guillot, H. Liu, Bariatric Surgery Associates with Nonalcoholic
513 Steatohepatitis/Hepatocellular Carcinoma Amelioration via SPP1 Suppression.
514 Metabolites 13, (2022).

515 14. S. Chen, Y. Jiang, X. Qi, P. Song, L. Tang, H. Liu, Bioinformatics analysis to obtain
516 critical genes regulated in subcutaneous adipose tissue after bariatric surgery. Adipocyte
517 11, 550-561 (2022).

518 15. M. Cerreto, F. Santopaolo, A. Gasbarrini, M. Pompili, F. R. Ponziani, Bariatric Surgery
519 and Liver Disease: General Considerations and Role of the Gut-Liver Axis. Nutrients 13,
520 (2021).

521 16. M. Thiele, I. F. Villesen, L. Niu, S. Johansen, K. Sulek, S. Nishijima, L. Van Espen, M.
522 Keller, M. Israelsen, T. Suvitaival, A. de Zawadzki, H. B. Juel, M. J. Brol, S. E. Stinson,
523 Y. Huang, M. C. Alvarez Silva, M. Kuhn, E. Anastasiadou, D. J. Leeming, M. Karsdal, J.

Matthijnssens, M. Arumugam, L. T. Dalgaard, C. Legido-Quigley, M. Mann, J. Trebicka, P. Bork, L. J. Jensen, T. Hansen, A. Krag, A. Krag, P. Bork, T. Hansen, M. Arumugam, J. Trebicka, M. Karsdal, E. Anastasiadou, H. Israelsen, H. O. Melberg, C. Legido-Quigley, M. Thiele, T. Hansen, M. Mann, J. Matthijnssens, A. Krag, Review: Opportunities and barriers for omics-based biomarker discovery in steatotic liver diseases. Journal of Hepatology.

17. V. Ratziu, M. Hompesch, M. Petitjean, C. Serdjebi, J. S. Iyer, A. V. Parwani, D. Tai, E. Bugianesi, K. Cusi, S. L. Friedman, E. Lawitz, M. Romero-Gomez, D. Schuppan, R. Loomba, V. Paradis, C. Behling, A. J. Sanyal, Artificial intelligence-assisted digital pathology for non-alcoholic steatohepatitis: current status and future directions. J Hepatol 80, 335-351 (2024).

18. M. Guilliams, J. Bonnardel, B. Haest, B. Vanderborght, C. Wagner, A. Remmerie, A. Bujko, L. Martens, T. Thone, R. Browaeys, F. F. De Ponti, B. Vanneste, C. Zwicker, F. R. Svedberg, T. Vanhalewyn, A. Goncalves, S. Lippens, B. Devriendt, E. Cox, G. Ferrero, V. Wittamer, A. Willaert, S. J. F. Kaptein, J. Neyts, K. Dallmeier, P. Geldhof, S. Casaert, B. Deplancke, P. Ten Dijke, A. Hoorens, A. Vanlander, F. Berrevoet, Y. Van Nieuwenhove, Y. Saeys, W. Saelens, H. Van Vlierberghe, L. Devisscher, C. L. Scott, Spatial proteogenomics reveals distinct and evolutionarily conserved hepatic macrophage niches. Cell 185, 379-396 e338 (2022).

19. M. Peiseler, B. Araujo David, J. Zindel, B. G. J. Surewaard, W. Y. Lee, F. Heymann, Y. Nusse, F. V. S. Castanheira, R. Shim, A. Guillot, A. Bruneau, J. Atif, C. Perciani, C. Ohland, P. Ganguli Mukherjee, A. Niehrs, R. Thuenauer, M. Altfeld, M. Amrein, Z. Liu, P. M. K. Gordon, K. McCoy, J. Deniset, S. MacParland, F. Ginhoux, F. Tacke, P. Kubes, Kupffer cell-like syncytia replenish resident macrophage function in the fibrotic liver. Science 381, eabq5202 (2023).

20. P. Ramachandran, R. Dobie, J. R. Wilson-Kanamori, E. F. Dora, B. E. P. Henderson, N. T. Luu, J. R. Portman, K. P. Matchett, M. Brice, J. A. Marwick, R. S. Taylor, M. Efremova, R. Vento-Tormo, N. O. Carragher, T. J. Kendall, J. A. Fallowfield, E. M. Harrison, D. J. Mole, S. J. Wigmore, P. N. Newsome, C. J. Weston, J. P. Iredale, F. Tacke, J. W. Pollard, C. P. Ponting, J. C. Marioni, S. A. Teichmann, N. C. Henderson, Resolving the fibrotic niche of human liver cirrhosis at single-cell level. Nature 575, 512-518 (2019).

21. M. Peiseler, R. Schwabe, J. Hampe, P. Kubes, M. Heikenwalder, F. Tacke, Immune mechanisms linking metabolic injury to inflammation and fibrosis in fatty liver disease - novel insights into cellular communication circuits. J Hepatol 77, 1136-1160 (2022).

22. J. T. Haas, L. Vonghia, D. A. Mogilenko, A. Verrijken, O. Molendi-Coste, S. Fleury, A. Deprince, A. Nikitin, E. Woitrain, L. Ducrocq-Geoffroy, S. Pic, B. Derudas, H. Dehondt, C. Gheeraert, L. Van Gaal, A. Driessen, P. Lefebvre, B. Staels, S. Francque, D. Dombrowicz, Transcriptional Network Analysis Implicates Altered Hepatic Immune Function in NASH development and resolution. Nat Metab 1, 604-614 (2019).

23. P. Lefebvre, F. Lalloyer, E. Bauge, M. Pawlak, C. Gheeraert, H. Dehondt, J. Vanhoutte, E. Woitrain, N. Hennuyer, C. Mazuy, M. Bobowski-Gerard, F. P. Zummo, B. Derudas, A. Driessen, G. Hubens, L. Vonghia, W. J. Kwanten, P. Michielsen, T. Vanwolleghem, J.

567 Eeckhoute, A. Verrijken, L. Van Gaal, S. Francque, B. Staels, Interspecies NASH disease
568 activity whole-genome profiling identifies a fibrogenic role of PPARalpha-regulated
569 dermatopontin. JCI Insight 2, (2017).

570 24. T. Puengel, H. Liu, A. Guillot, F. Heymann, F. Tacke, M. Peiseler, Nuclear Receptors
571 Linking Metabolism, Inflammation, and Fibrosis in Nonalcoholic Fatty Liver Disease. Int
572 J Mol Sci 23, (2022).

573 25. S. Kamata, A. Honda, R. Ishikawa, M. Akahane, A. Fujita, C. Kaneko, S. Miyawaki, Y.
574 Habu, Y. Shiiyama, K. Uchii, Y. Machida, T. Oyama, I. Ishii, Functional and Structural
575 Insights into the Human PPARalpha/delta/gamma Targeting Preferences of Anti-NASH
576 Investigational Drugs, Lanifibranor, Seladelpar, and Elafibranor. Antioxidants (Basel) 12,
577 (2023).

578 26. F. Tacke, T. Puengel, R. Loomba, S. L. Friedman, An integrated view of anti-
579 inflammatory and antifibrotic targets for the treatment of NASH. J Hepatol 79, 552-566
580 (2023).

581 27. P. Hu, K. Li, X. Peng, Y. Kan, H. Li, Y. Zhu, Z. Wang, Z. Li, H. Y. Liu, D. Cai, Nuclear
582 Receptor PPARalpha as a Therapeutic Target in Diseases Associated with Lipid
583 Metabolism Disorders. Nutrients 15, (2023).

584 28. L. Gong, F. Wei, F. J. Gonzalez, G. Li, Hepatic fibrosis: Targeting peroxisome
585 proliferator-activated receptor alpha from mechanism to medicines. Hepatology 78,
586 1625-1653 (2023).

587 29. S. Lefere, T. Puengel, J. Hundertmark, C. Penners, A. K. Frank, A. Guillot, K. de
588 Muynck, F. Heymann, V. Adarbes, E. Defrene, C. Estivalet, A. Geerts, L. Devisscher, G.
589 Wettstein, F. Tacke, Differential effects of selective- and pan-PPAR agonists on
590 experimental steatohepatitis and hepatic macrophages(☆). J Hepatol 73, 757-770 (2020).

591 30. S. Kamata, A. Honda, I. Ishii, Current Clinical Trial Status and Future Prospects of
592 PPAR-Targeted Drugs for Treating Nonalcoholic Fatty Liver Disease. Biomolecules 13,
593 (2023).

594 31. J. Vonderlin, T. Chavakis, M. Sieweke, F. Tacke, The Multifaceted Roles of
595 Macrophages in NAFLD Pathogenesis. Cell Mol Gastroenterol Hepatol 15, 1311-1324
596 (2023).

597 32. M. S. Kohlhepp, H. Liu, F. Tacke, A. Guillot, The contradictory roles of macrophages in
598 non-alcoholic fatty liver disease and primary liver cancer-Challenges and opportunities.
599 Front Mol Biosci 10, 1129831 (2023).

600 33. S. Lefere, F. Tacke, Macrophages in obesity and non-alcoholic fatty liver disease:
601 Crosstalk with metabolism. JHEP Rep 1, 30-43 (2019).

602 34. P. X. Ji, Y. X. Chen, X. X. Ni, Q. Miao, J. Hua, Effect of triggering receptor expressed
603 on myeloid cells 2-associated alterations on lipid metabolism in macrophages in the
604 development of non-alcoholic fatty liver disease. J Gastroenterol Hepatol 39, 369-380
605 (2024).

606 35. Y. Yuan, Y. Zhang, X. Lu, J. Li, M. Wang, W. Zhang, M. Zheng, Z. Sun, Y. Xing, Y. Li,
607 Y. Qu, Y. Jiao, H. Han, C. Xie, T. Mao, Novel insights into macrophage

608 immunometabolism in nonalcoholic steatohepatitis. Int Immunopharmacol 131, 111833
609 (2024).

610 36. J. Zhao, K. Wei, P. Jiang, C. Chang, L. Xu, L. Xu, Y. Shi, S. Guo, Y. Xue, D. He,
611 Inflammatory Response to Regulated Cell Death in Gout and Its Functional Implications.
612 Front Immunol 13, 888306 (2022).

613 37. Y. Wen, J. Lambrecht, C. Ju, F. Tacke, Hepatic macrophages in liver homeostasis and
614 diseases-diversity, plasticity and therapeutic opportunities. Cell Mol Immunol 18, 45-56
615 (2021).

616 38. F. Tacke, Targeting hepatic macrophages to treat liver diseases. J Hepatol 66, 1300-1312
617 (2017).

618 39. C. Ju, F. Tacke, Hepatic macrophages in homeostasis and liver diseases: from
619 pathogenesis to novel therapeutic strategies. Cell Mol Immunol 13, 316-327 (2016).

620 40. S. Jordan, N. Tung, M. Casanova-Acebes, C. Chang, C. Cantoni, D. Zhang, T. H. Wirtz,
621 S. Naik, S. A. Rose, C. N. Brocker, A. Gainullina, D. Hornburg, S. Horng, B. B. Maier,
622 P. Cravedi, D. LeRoith, F. J. Gonzalez, F. Meissner, J. Ochando, A. Rahman, J. E.
623 Chipuk, M. N. Artyomov, P. S. Frenette, L. Piccio, M. L. Berres, E. J. Gallagher, M.
624 Merad, Dietary Intake Regulates the Circulating Inflammatory Monocyte Pool. Cell 178,
625 1102-1114 e1117 (2019).

626 41. L. Hammerich, F. Tacke, Hepatic inflammatory responses in liver fibrosis. Nat Rev
627 Gastroenterol Hepatol 20, 633-646 (2023).

628 42. J. Aron-Wisnewsky, J. Dore, K. Clement, The importance of the gut microbiota after
629 bariatric surgery. Nat Rev Gastroenterol Hepatol 9, 590-598 (2012).

630 43. G. Musso, R. Gambino, M. Cassader, Interactions between gut microbiota and host
631 metabolism predisposing to obesity and diabetes. Annu Rev Med 62, 361-380 (2011).

632 44. C. W. le Roux, S. J. Aylwin, R. L. Batterham, C. M. Borg, F. Coyle, V. Prasad, S.
633 Shurey, M. A. Ghatei, A. G. Patel, S. R. Bloom, Gut hormone profiles following bariatric
634 surgery favor an anorectic state, facilitate weight loss, and improve metabolic parameters.
635 Ann Surg 243, 108-114 (2006).

636 45. S. G. Koulas, C. K. Stefanou, S. K. Stefanou, K. Tepelenis, N. Zikos, K. Tepetes, A.
637 Kapsoritakis, Gut Microbiota in Patients with Morbid Obesity Before and After Bariatric
638 Surgery: a Ten-Year Review Study (2009-2019). Obes Surg 31, 317-326 (2021).

639 46. D. J. Pournaras, C. Glicksman, R. P. Vincent, S. Kuganolipava, J. Alaghband-Zadeh, D.
640 Mahon, J. H. Bekker, M. A. Ghatei, S. R. Bloom, J. R. Walters, R. Welbourn, C. W. le
641 Roux, The role of bile after Roux-en-Y gastric bypass in promoting weight loss and
642 improving glycaemic control. Endocrinology 153, 3613-3619 (2012).

643 47. E. Talavera-Urquijo, M. Beisani, J. M. Balibrea, J. C. Alverdy, Is bariatric surgery
644 resolving NAFLD via microbiota-mediated bile acid ratio reversal? A comprehensive
645 review. Surg Obes Relat Dis 16, 1361-1369 (2020).

646 48. F. Zhou, T. Mai, Z. Wang, Z. Zeng, J. Shi, F. Zhang, N. Kong, H. Jiang, L. Guo, M. Xu,
647 J. Lin, The improvement of intestinal dysbiosis and hepatic metabolic dysfunction in

648 dextran sulfate sodium-induced colitis mice: effects of curcumin. J Gastroenterol Hepatol
649 38, 1333-1345 (2023).

650 49. Y. S. Park, K. Ahn, K. Yun, J. Jeong, K. W. Baek, J. Lee, H. H. Kim, K. Han, Y. J. Ahn,
651 Alterations in gastric and gut microbiota following sleeve gastrectomy in high-fat diet-
652 induced obese rats. Sci Rep 13, 21294 (2023).

653 50. J. Paris, N. C. Henderson, Liver zonation, revisited. Hepatology 76, 1219-1230 (2022).

654 51. T. Martini, F. Naef, J. S. Tchorz, Spatiotemporal Metabolic Liver Zonation and
655 Consequences on Pathophysiology. Annu Rev Pathol 18, 439-466 (2023).

656 52. Y. Hoshida, S. M. Nijman, M. Kobayashi, J. A. Chan, J. P. Brunet, D. Y. Chiang, A.
657 Villanueva, P. Newell, K. Ikeda, M. Hashimoto, G. Watanabe, S. Gabriel, S. L.
658 Friedman, H. Kumada, J. M. Llovet, T. R. Golub, Integrative transcriptome analysis
659 reveals common molecular subclasses of human hepatocellular carcinoma. Cancer Res
660 69, 7385-7392 (2009).

661 53. X. Qi, X. Li, Y. Jiao, S. Chen, P. Song, Z. Qian, L. Tang, The Effects of Antral
662 Preservation and Antral Resection on Body Composition, Glycemic Control and Bone
663 Mineral Density Following Vertical Sleeve Gastrectomy in C57BL/6J Mice with Obesity
664 and Type 2 Diabetes. Diabetes Metab Syndr Obes 15, 297-305 (2022).

665 54. M. Albersheim, W. Fedje-Johnston, C. Carlson, S. P. Arnoczky, F. Toth, K. Shea, L.
666 Harper, A. Rendahl, M. Tompkins, Cell Count and Cell Density Decrease as Age
667 Increases in Cadaveric Pediatric Medial Menisci. Arthrosc Sports Med Rehabil 5, 100795
668 (2023).

669 55. M. Slyper, C. B. M. Porter, O. Ashenberg, J. Waldman, E. Drokhlyansky, I. Wakiro, C.
670 Smillie, G. Smith-Rosario, J. Wu, D. Dionne, S. Vigneau, J. Jane-Valbuena, T. L. Tickle,
671 S. Napolitano, M. J. Su, A. G. Patel, A. Karlstrom, S. Gritsch, M. Nomura, A. Waghray,
672 S. H. Gohil, A. M. Tsankov, L. Jerby-Arnon, O. Cohen, J. Klughammer, Y. Rosen, J.
673 Gould, L. Nguyen, M. Hofree, P. J. Tramontozzi, B. Li, C. J. Wu, B. Izar, R. Haq, F. S.
674 Hodi, C. H. Yoon, A. N. Hata, S. J. Baker, M. L. Suva, R. Bueno, E. H. Stover, M. R.
675 Clay, M. A. Dyer, N. B. Collins, U. A. Matulonis, N. Wagle, B. E. Johnson, A. Rotem,
676 O. Rozenblatt-Rosen, A. Regev, A single-cell and single-nucleus RNA-Seq toolbox for
677 fresh and frozen human tumors. Nat Med 26, 792-802 (2020).

678 56. S. Slovin, A. Carissimo, F. Panariello, A. Grimaldi, V. Bouche, G. Gambardella, D.
679 Cacchiarelli, Single-Cell RNA Sequencing Analysis: A Step-by-Step Overview. Methods
680 Mol Biol 2284, 343-365 (2021).

681 57. S. Jin, C. F. Guerrero-Juarez, L. Zhang, I. Chang, R. Ramos, C. H. Kuan, P. Myung, M.
682 V. Plikus, Q. Nie, Inference and analysis of cell-cell communication using CellChat. Nat
683 Commun 12, 1088 (2021).

684 58. X. Qiu, Q. Mao, Y. Tang, L. Wang, R. Chawla, H. A. Pliner, C. Trapnell, Reversed graph
685 embedding resolves complex single-cell trajectories. Nat Methods 14, 979-982 (2017).

686 59. D. Unsihuay, D. Mesa Sanchez, J. Laskin, Quantitative Mass Spectrometry Imaging of
687 Biological Systems. Annu Rev Phys Chem 72, 307-329 (2021).

60. J. Calderaro, N. Ghaffari Laleh, Q. Zeng, P. Maille, L. Favre, A. Pujals, C. Klein, C. Bazille, L. R. Heij, A. Uguen, T. Luedde, L. Di Tommaso, A. Beaufrere, A. Chatain, D. Gastineau, C. T. Nguyen, H. Nguyen-Canh, K. N. Thi, V. Gnemmi, R. P. Graham, F. Charlotte, D. Wendum, M. Vij, D. S. Allende, F. Aucejo, A. Diaz, B. Riviere, A. Herrero, K. Evert, D. F. Calvisi, J. Augustin, W. Q. Leow, H. H. W. Leung, E. Boleslawski, M. Rela, A. Francois, A. W. Cha, A. Forner, M. Reig, M. Allaire, O. Scatton, D. Chatelain, C. Boulagnon-Rombi, N. Sturm, B. Menahem, E. Frouin, D. Tougeron, C. Tournigand, E. Kempf, H. Kim, M. Ningarhari, S. Michalak-Provost, P. Gopal, R. Brustia, E. Vibert, K. Schulze, D. F. Ruther, S. A. Weidemann, R. Rhaiem, J. M. Pawlotsky, X. Zhang, A. Luciani, S. Mule, A. Laurent, G. Amaddeo, H. Regnault, E. De Martin, C. Sempoux, P. Navale, M. Westerhoff, R. C. Lo, J. Bednarsch, A. Gouw, C. Guettier, M. Lequoy, K. Harada, P. Sripongpun, P. Wetwittayaklang, N. Lomenie, J. Tantipisit, A. Kaewdech, J. Shen, V. Paradis, S. Caruso, J. N. Kather, Deep learning-based phenotyping reclassifies combined hepatocellular-cholangiocarcinoma. Nat Commun 14, 8290 (2023).

61. Q. Zeng, C. Klein, S. Caruso, P. Maille, D. S. Allende, B. Minguez, M. Iavarone, M. Ningarhari, A. Casadei-Gardini, F. Pedica, M. Rimini, R. Perbellini, C. Boulagnon-Rombi, A. Heurgue, M. Maggioni, M. Rela, M. Vij, S. Baulande, P. Legoix, S. Lameiras, H.-A. s. group, L. Bruges, V. Gnemmi, J. C. Nault, C. Campani, H. Rhee, Y. N. Park, M. Inarrairaegui, G. Garcia-Porrero, J. Argemi, B. Sangro, A. D'Alessio, B. Scheiner, D. J. Pinato, M. Pinter, V. Paradis, A. Beaufrere, S. Peter, L. Rimassa, L. Di Tommaso, A. Vogel, S. Michalak, J. Boursier, N. Lomenie, M. Ziol, J. Calderaro, Artificial intelligence-based pathology as a biomarker of sensitivity to atezolizumab-bevacizumab in patients with hepatocellular carcinoma: a multicentre retrospective study. Lancet Oncol 24, 1411-1422 (2023).

62. Q. Zeng, C. Klein, S. Caruso, P. Maille, N. G. Laleh, D. Sommacale, A. Laurent, G. Amaddeo, D. Gentien, A. Rapinat, H. Regnault, C. Charpy, C. T. Nguyen, C. Tournigand, R. Brustia, J. M. Pawlotsky, J. N. Kather, M. C. Maiuri, N. Lomenie, J. Calderaro, Artificial intelligence predicts immune and inflammatory gene signatures directly from hepatocellular carcinoma histology. J Hepatol 77, 116-127 (2022).

63. H. S. Muti, C. M. L. Loeffler, A. Echle, L. R. Heij, R. D. Bülow, J. Krause, L. Broderius, J. M. Niehues, G. Liapi, P. Boor, H. I. Grabsch, S. E. Kochanny, A. T. Pearson, J. N. Kather. (2020).

64. S. Han, I. Y. Kwak, Mastering data visualization with Python: practical tips for researchers. J Minim Invasive Surg 26, 167-175 (2023).

65. K. Ito, D. Murphy, Application of ggplot2 to Pharmacometric Graphics. CPT Pharmacometrics Syst Pharmacol 2, e79 (2013).

Acknowledgments: The authors thank Shanghai OE Biotech CO., Ltd. and Shanghai Luming Biological Technology Co., Ltd. for the access to the MobiNova single-cell system and AFADESI-MSI platforms. Xiurong Cai and Hanyang Liu were funded by China Scholarship Council Foundation.

Funding:

National Nature Science Foundation of China (82300730)

Changzhou Health Commission of China (CZQM2022007 and QN202121)

Changzhou Science and Technology Bureau of China (CJ20220142)

Changzhou Medical Center of Nanjing Medical University (CZKYCMCB202221)

German Research Foundation (DFG Ta434/8-1, SFB/TRR 296 and CRC1382, Project-ID 403224013).

Author contributions:

Conceptualization: HL, SC
Methodology: SC, QZ, XC, JX, PS, CK
Investigation: SC, QZ, XC, JX, PS, CK, LT
Visualization: SFB, MJM, JLS, EH
Funding acquisition: HL, FT, AG
Project administration: HL, FT, AG
Supervision: HL, AG
Writing – original draft: HL, SC, QZ
Writing – review & editing: HL, FT, AG

Competing interests: FT's lab has received research funding from Gilead, AstraZeneca and MSD (funding to the institution). FT has received honoraria for consulting or lectures from AstraZeneca, Gilead, AbbVie, BMS, Boehringer, Madrigal, Intercept, Falk, Inventiva, MSD, GSK, Orphalan, Merz, Pfizer, Alnylam, CSL Behring, Novo Nordisk, Sanofi and Novartis.

Data and materials availability: Raw and processed data of sc/sn-RNA sequencing analysis can be obtained from the GEO database (https://www.ncbi.nlm.nih.gov/geo/) with the reference number GSE254841. Raw data of spatial metabolomics can be obtained from the OMIX, China National Center for Bioinformation (https://ngdc.cncb.ac.cn/omix/) with the reference number OMIX005793. Technical materials for the deep-learning-based image analysis model may be provided by the corresponding authors upon reasonable requests.

Figures

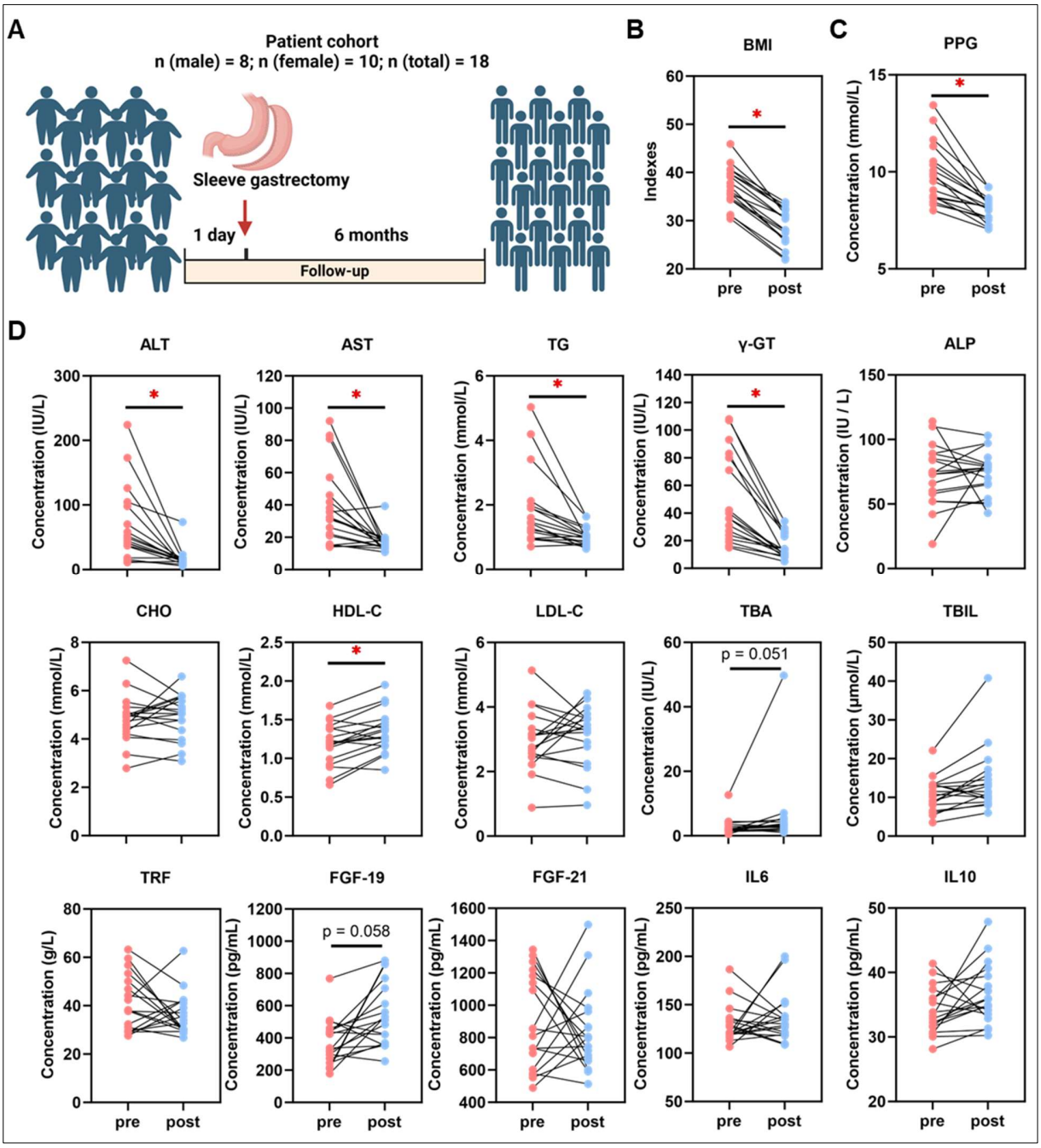

Figure 1. Sleeve gastrectomy induces weight loss and MASLD amelioration in patients. (A) Description of the patient cohort receiving SG. Comparisons of (B) BMI and (C) PPG, together with (D) ALT, AST, TG, γ-GT, ALP, CHO, HDL-C, LDL-C, TBA, TBIL, TRF, FGF-19, FGF-21, IL-6 and IL-10 in patients between one day pre-SG and 6 months post-SG. Abbreviations: SG: sleeve gastrectomy; BMI: body mass index; PPG: postprandial blood glucose; AST: aspartate aminotransferase; ALT: alanine aminotransferase; γ-GT: gamma-glutamyltransferase; TG, triglycerides; CHO, cholesterol; HDL-C, high-density

779 lipoprotein cholesterol; LDL-C, low-density lipoprotein cholesterol; TBIL, total bilirubin;
780 ALP, alkaline phosphatase; TBA, total bile acid. TRF: transferrin; IL: interleukin; FGF,
781 fibroblast growth factor. The paired t-test was performed. '*' represents '$p < 0.05$' and
782 statistical significance.

783

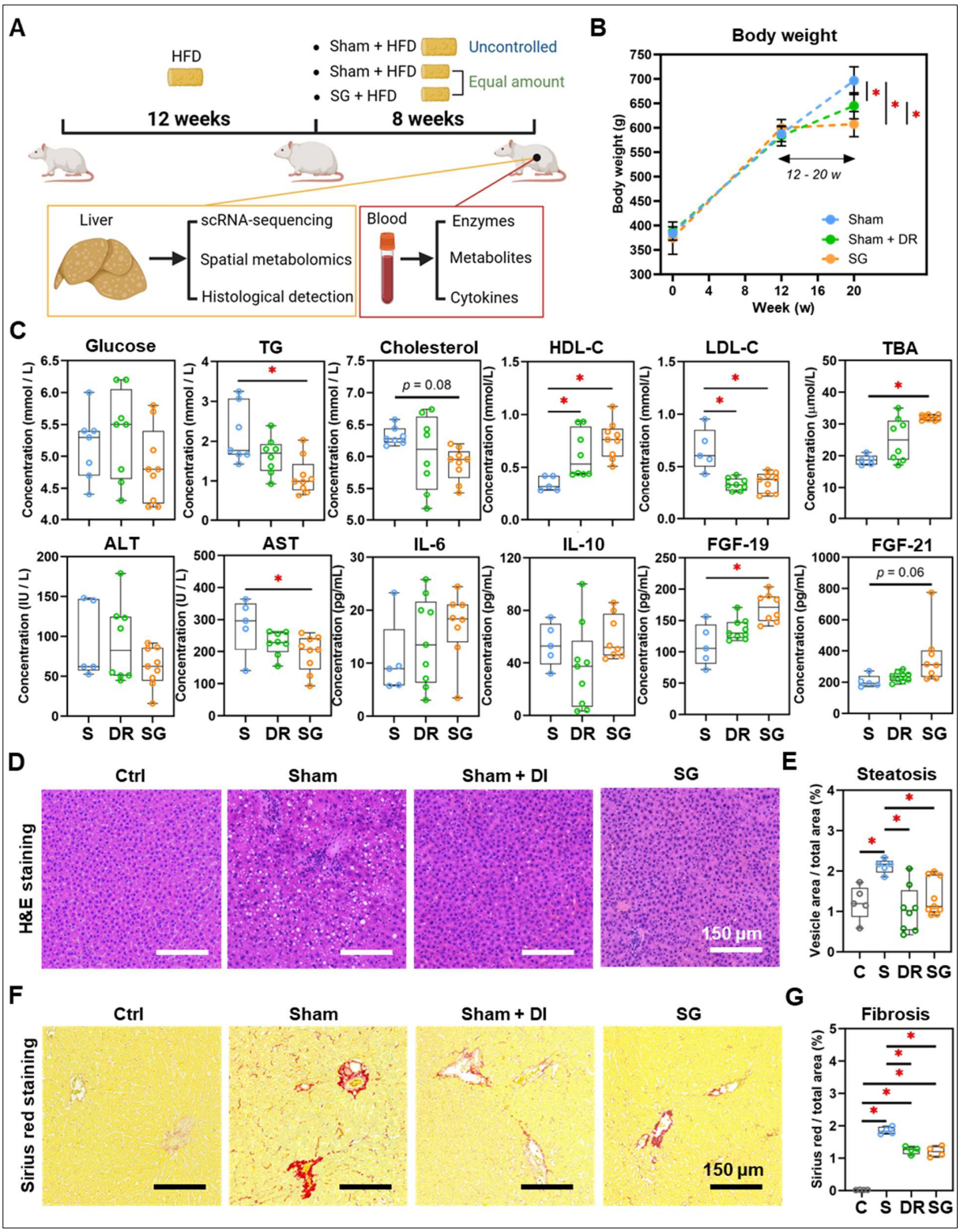

Figure 2. Sleeve gastrectomy and dietary restriction induce weight loss and MASLD amelioration in rat models. (A) The technical scheme of the rat MASLD model and surgical interventions. (B) Body weight was recorded for 20 weeks of modeling. (C)

Serological indexes (glucose, triglycerides, cholesterol, HDL-C, LDL-C, TBA, ALT, AST, ALP, IL-6, IL-10, FGF-19 and FGF-21) were measured. (D) H&E-stained rat liver tissue and (E) quantification of steatosis (area of hepatocyte lipid vesicles) from Ctrl, Sham, Sham + DR and SG groups. (F) Sirius red-stained rat liver tissue and (G) quantification of fibrosis from Ctrl, Sham, Sham + DR and SG groups. Abbreviations: Sham/S: sham surgery; DR: dietary restriction; SG: sleeve gastrectomy; Ctrl: control fed a normal diet; HDL-C: density lipoprotein-cholesterol, LDL-C: low-density lipoprotein-cholesterol; TG: triglycerides; TBA: total bile acids, ALT: alanine transaminase; AST: aspartate aminotransferase; ALP: alkaline phosphatase; IL: interleukin; FGF: fibroblast growth factor. The one-way ANOVA test was performed. '*' represents '$p < 0.05$' and statistical significance.

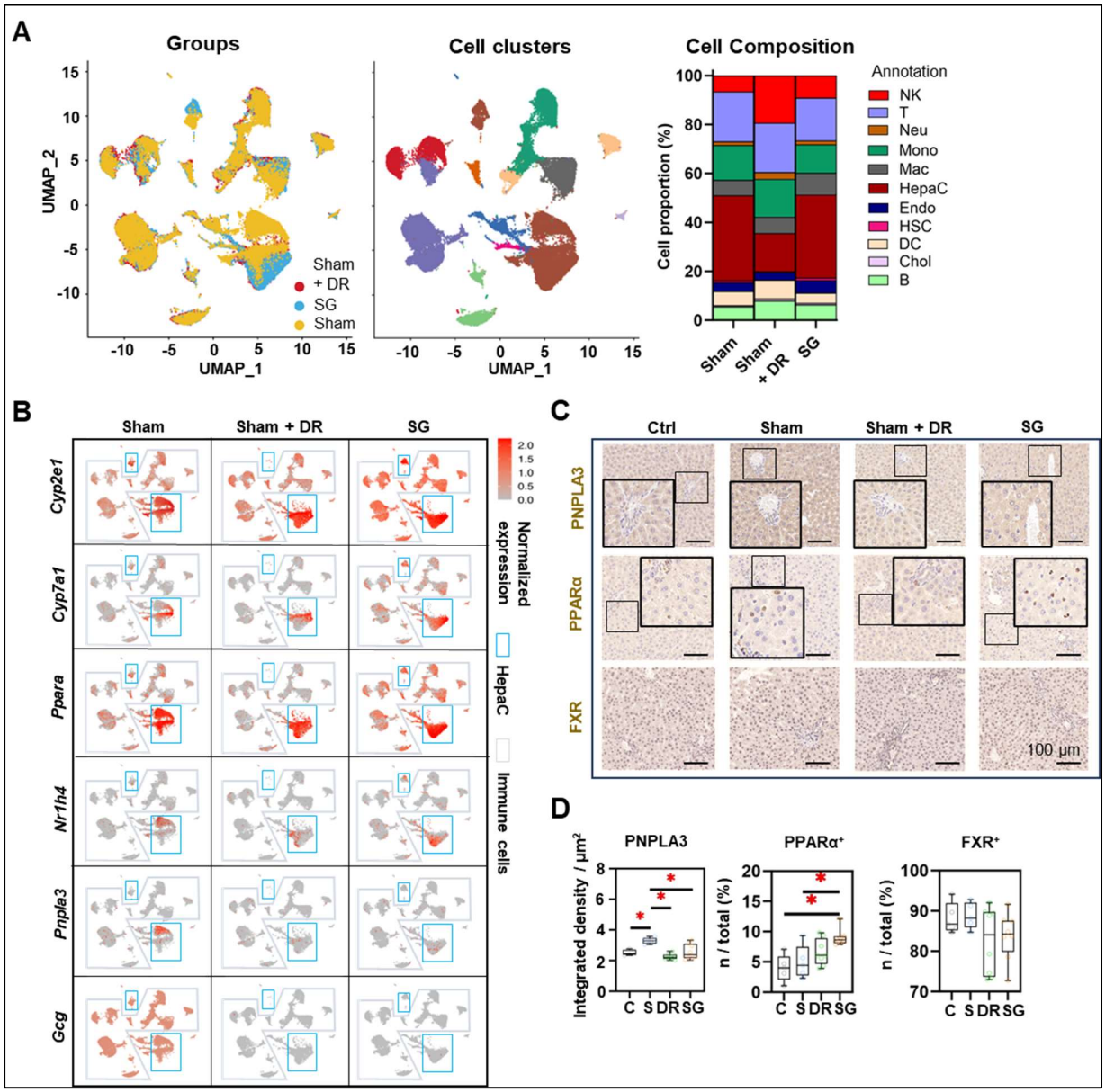

801 **Figure 3. Sleeve gastrectomy improves hepatic metabolism according to sc/sn-**
802 **transcriptome analysis and in-situ exploration.** (A) UMAPs describe the distribution
803 of B cells, cholangiocytes, DCs, endothelial cells, hepatic stellate cells, hepatocytes,
804 macrophages, monocytes, neutrophils, T cells and NK cells. Histograms describing cell
805 proportions. (B) Gene expressions of Cyp2e1, Cyp7a1, Ppara, Nr1h4, Pnpla3 and Gcg
806 were illustrated on rat liver cells upon Sham, Sham + DR and SG. Protein levels of
807 PNPLA3, PPARα and FXR were illustrated (C) and quantified (D) on rat liver tissue of
808 Ctrl, Sham, Sham + DR and SG groups. Abbreviations: Ctrl: control fed a normal diet;
809 Sham: sham surgery; DR: dietary restriction; SG: sleeve gastrectomy; PPAR: peroxisome
810 proliferator-activated receptor; PNPLA: patatin-like phospholipase domain-containing
811 protein; FXR: farnesoid X receptor; CK: cytokeratin; IL: interleukin; DC: dendritic cells;
812 NK: natural killer cells; B: B lymphocytes; T: T lymphocytes; Neu: neutrophils; Mac:
813 macrophages; Mono: monocytes: Endo: endothelial cells; HSC: hepatic stellate cells;
814 Chol: cholangiocytes; HepaC: hepatocytes.

815

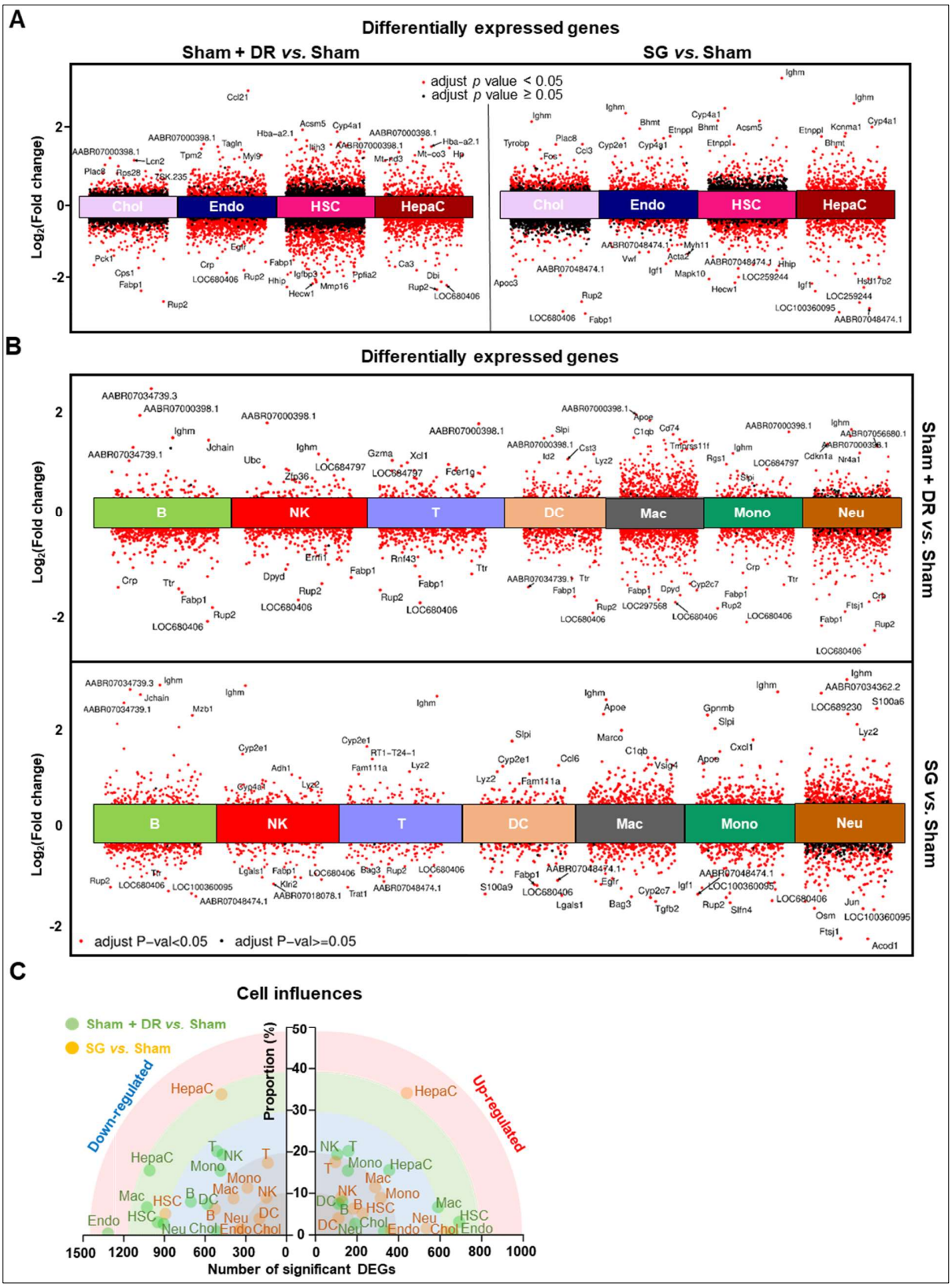
A
Differentially expressed genes
Sham + DR vs. Sham
SG vs. Sham
adjust p value < 0.05
adjust p value ≥ 0.05
Log2(Fold change)
Chol
Endo
HSC
HepaC
B
Differentially expressed genes
Sham + DR vs. Sham
SG vs. Sham
B
NK
T
DC
Mac
Mono
Neu
adjust P-val<0.05
adjust P-val>=0.05
C
Cell influences
Sham + DR vs. Sham
SG vs. Sham
Down-regulated
Up-regulated
Proportion (%)
Number of significant DEGs

816

817 **Figure 4. Sc/sn-transcriptome analysis illustrates differentially expressed genes in diverse**
818 **liver cells.** (A & B) Differentially expressed genes of hepatocytes, cholangiocytes,
819 endothelial cells, hepatic stellate cells, B, T, NK, DCs, macrophages, monocytes and
820 neutrophils (Sham + DR vs. Sham and SG vs. Sham) were illustrated in volcano plots.
821 (C) Transcriptomic influences of hepatocytes, cholangiocytes, endothelial cells, hepatic
822 stellate cells, B, T, NK, DCs, macrophages, monocytes and neutrophils in the liver were
823 assessed with DEG numbers and cell proportion of total cells Abbreviations: Sham: sham
824 surgery; DR: dietary restriction; SG: sleeve gastrectomy; DC: dendritic cells; NK: natural
825 killers; B: B lymphocytes; T: T lymphocytes; Neu: neutrophils; Mac: macrophages;
826 Mono: monocytes: Endo: endothelial cells; HSC: hepatic stellate cells; Chol:
827 cholangiocytes; HepaC: hepatocytes; DEG: differentially expressed gene. The one-way
828 ANOVA test was performed. 'Adjust $p < 0.05$' represents statistical significance.

829

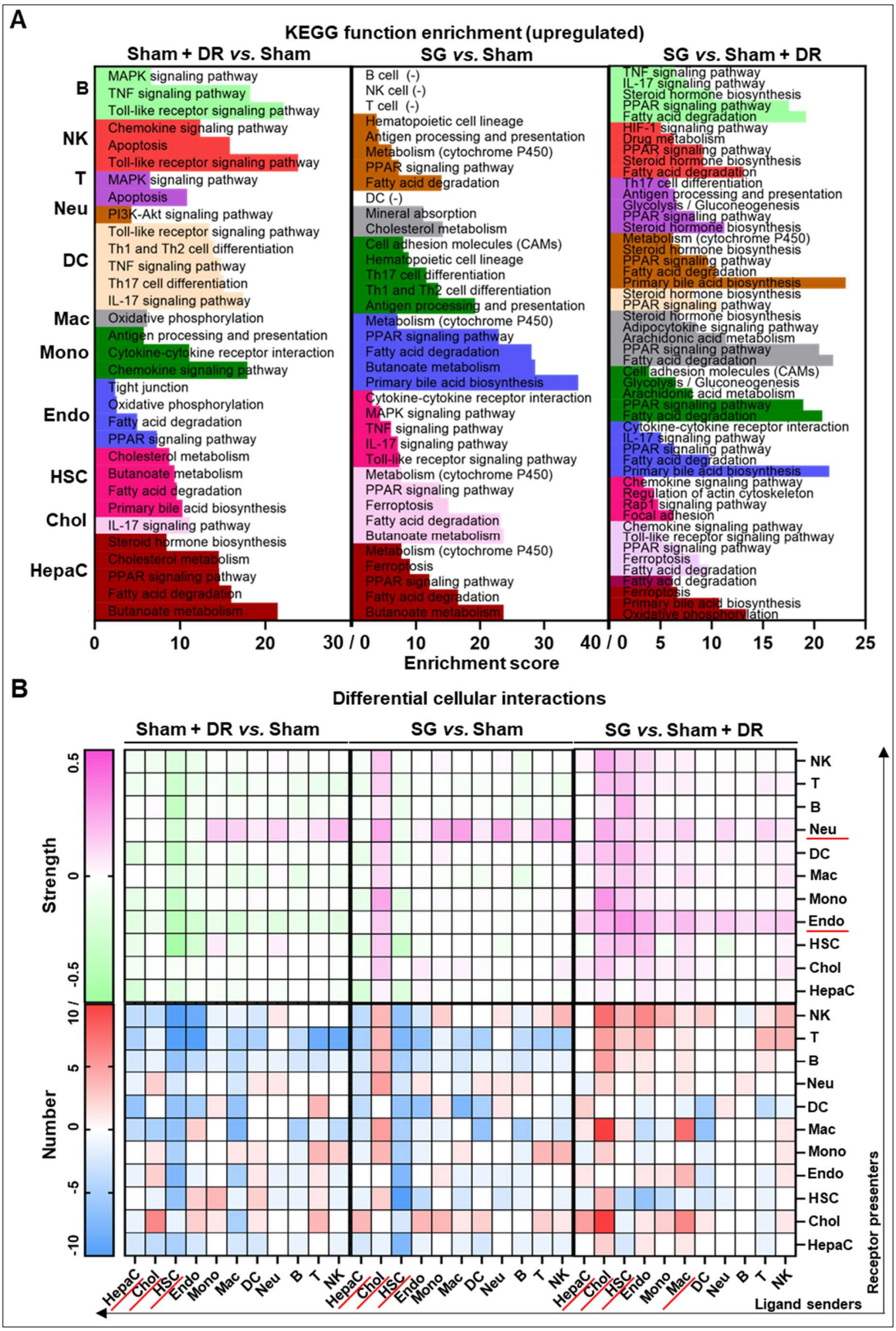
A
KEGG function enrichment (upregulated)
Sham + DR vs. Sham
SG vs. Sham
SG vs. Sham + DR
B
MAPK signaling pathway
TNF signaling pathway
Toll-like receptor signaling pathway
Chemokine signaling pathway
Apoptosis
Toll-like receptor signaling pathway
MAPK signaling pathway
Apoptosis
PI3K-Akt signaling pathway
Toll-like receptor signaling pathway
Th1 and Th2 cell differentiation
TNF signaling pathway
Th17 cell differentiation
IL-17 signaling pathway
Oxidative phosphorylation
Antigen processing and presentation
Cytokine-cytokine receptor interaction
Chemokine signaling pathway
Tight junction
Oxidative phosphorylation
Fatty acid degradation
PPAR signaling pathway
Cholesterol metabolism
Butanoate metabolism
Fatty acid degradation
Primary bile acid biosynthesis
IL-17 signaling pathway
Steroid hormone biosynthesis
Cholesterol metabolism
PPAR signaling pathway
Fatty acid degradation
Butanoate metabolism
B cell (-)
NK cell (-)
T cell (-)
Hematopoietic cell lineage
Antigen processing and presentation
Metabolism (cytochrome P450)
PPAR signaling pathway
Fatty acid degradation
DC (-)
Mineral absorption
Cholesterol metabolism
Cell adhesion molecules (CAMs)
Hematopoietic cell lineage
Th17 cell differentiation
Th1 and Th2 cell differentiation
Antigen processing and presentation
Metabolism (cytochrome P450)
PPAR signaling pathway
Fatty acid degradation
Butanoate metabolism
Primary bile acid biosynthesis
Cytokine-cytokine receptor interaction
MAPK signaling pathway
TNF signaling pathway
IL-17 signaling pathway
Toll-like receptor signaling pathway
Metabolism (cytochrome P450)
PPAR signaling pathway
Ferroptosis
Fatty acid degradation
Butanoate metabolism
Metabolism (cytochrome P450)
Ferroptosis
PPAR signaling pathway
Fatty acid degradation
Butanoate metabolism
TNF signaling pathway
IL-17 signaling pathway
Steroid hormone biosynthesis
PPAR signaling pathway
Fatty acid degradation
HIF-1 signaling pathway
Drug metabolism
PPAR signaling pathway
Steroid hormone biosynthesis
Fatty acid degradation
Th17 cell differentiation
Antigen processing and presentation
Glycolysis / Gluconeogenesis
PPAR signaling pathway
Steroid hormone biosynthesis
Metabolism (cytochrome P450)
Steroid hormone biosynthesis
PPAR signaling pathway
Fatty acid degradation
Primary bile acid biosynthesis
Steroid hormone biosynthesis
PPAR signaling pathway
Steroid hormone biosynthesis
Adipocytokine signaling pathway
Arachidonic acid metabolism
PPAR signaling pathway
Fatty acid degradation
Cell adhesion molecules (CAMs)
Glycolysis / Gluconeogenesis
Arachidonic acid metabolism
PPAR signaling pathway
Fatty acid degradation
Cytokine-cytokine receptor interaction
IL-17 signaling pathway
PPAR signaling pathway
Fatty acid degradation
Primary bile acid biosynthesis
Chemokine signaling pathway
Regulation of actin cytoskeleton
Rap1 signaling pathway
Focal adhesion
Chemokine signaling pathway
Toll-like receptor signaling pathway
PPAR signaling pathway
Ferroptosis
Fatty acid degradation
Fatty acid degradation
Ferroptosis
Primary bile acid biosynthesis
Oxidative phosphorylation
B
NK
T
Neu
DC
Mac
Endo
HSC
Chol
HepaC
0
10
20
30 / 0
10
20
30
40 / 0
5
10
15
20
25
Enrichment score
Differential cellular interactions
Sham + DR vs. Sham
SG vs. Sham
SG vs. Sham + DR
Strength
0.5
0
-0.5
Number
10 /
5
0
-5
-10
Receptor presenters
Ligand senders

Figure 5. Sc/sn-transcriptome analysis illustrates up-regulated enriched pathways and cellular interactions in diverse liver cells. Significantly up-regulated (A) KEGG signaling pathways and (B) cellular interactions (numbers and strength) in hepatocytes, cholangiocytes, endothelial cells, hepatic stellate cells, B, T, NK, DCs, macrophages, monocytes and neutrophils were illustrated (Sham + DR vs. Sham and SG vs. Sham). Abbreviations: Sham: sham surgery; DR: dietary restriction; SG: sleeve gastrectomy; HepaC: hepatocytes; Chol: cholangiocytes; HSC: hepatic stellate cells; Endo: endothelial cells; Mono: monocytes; Mac: macrophages; DC: dendritic cells; Neu: neutrophils; NK: natural killer cells; B: B lymphocytes; T: T lymphocytes; KEGG: Kyoto encyclopedia of genes and genomes. The one-way ANOVA test was performed.

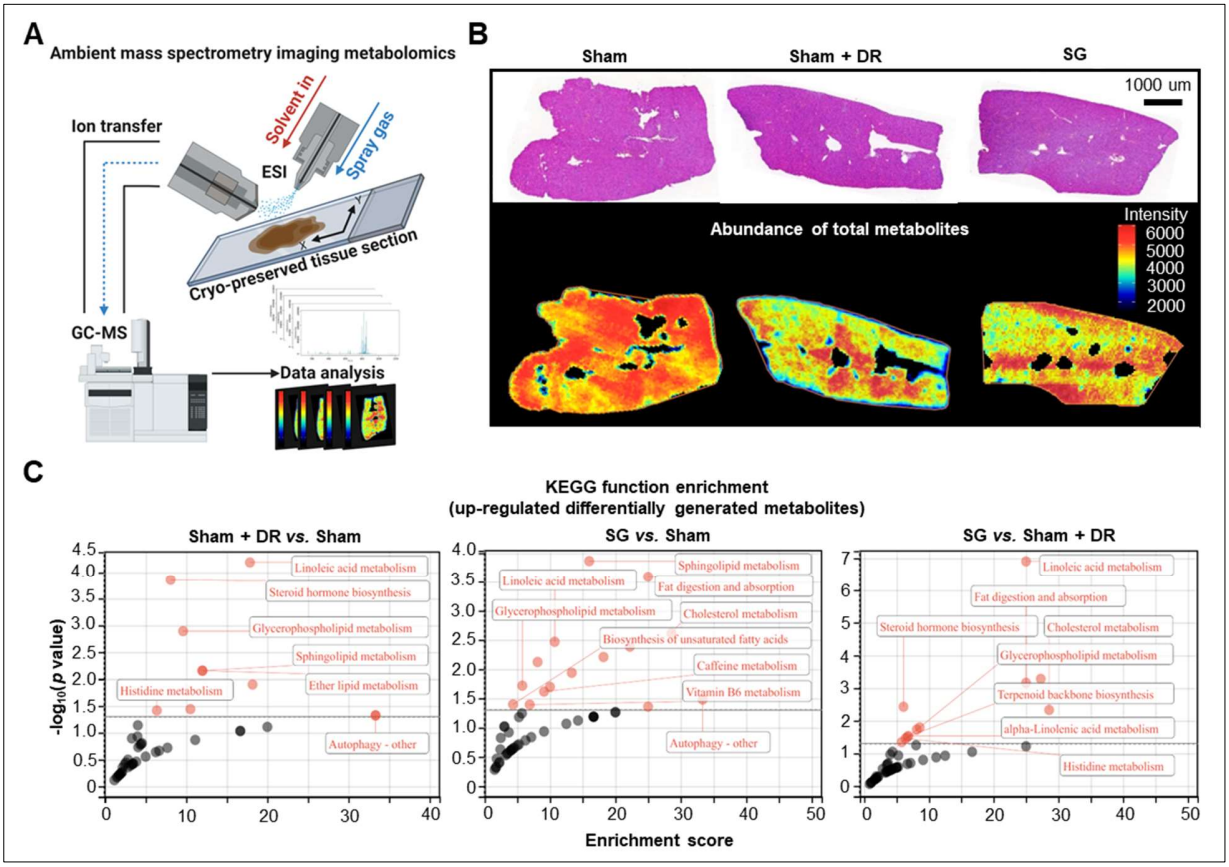

Figure 6. Sleeve gastrectomy and dietary restriction enhance metabolic capacities in steatotic livers. (A) Technical scheme of the ambient mass spectrometry imaging metabolomics method. (B) H&E-stained rat liver sample section was mapped with the abundance of total metabolites in Sham, Sham + DR and SG groups. (C) Function enrichment of upregulated differentially generated metabolites (Sham + DR vs. Sham, SG vs. Sham and SG vs. Sham + DR) was analyzed based on the KEGG database. Abbreviations: Sham: sham surgery; DR: dietary restriction; SG: sleeve gastrectomy; KEGG: Kyoto encyclopedia of genes and genomes.

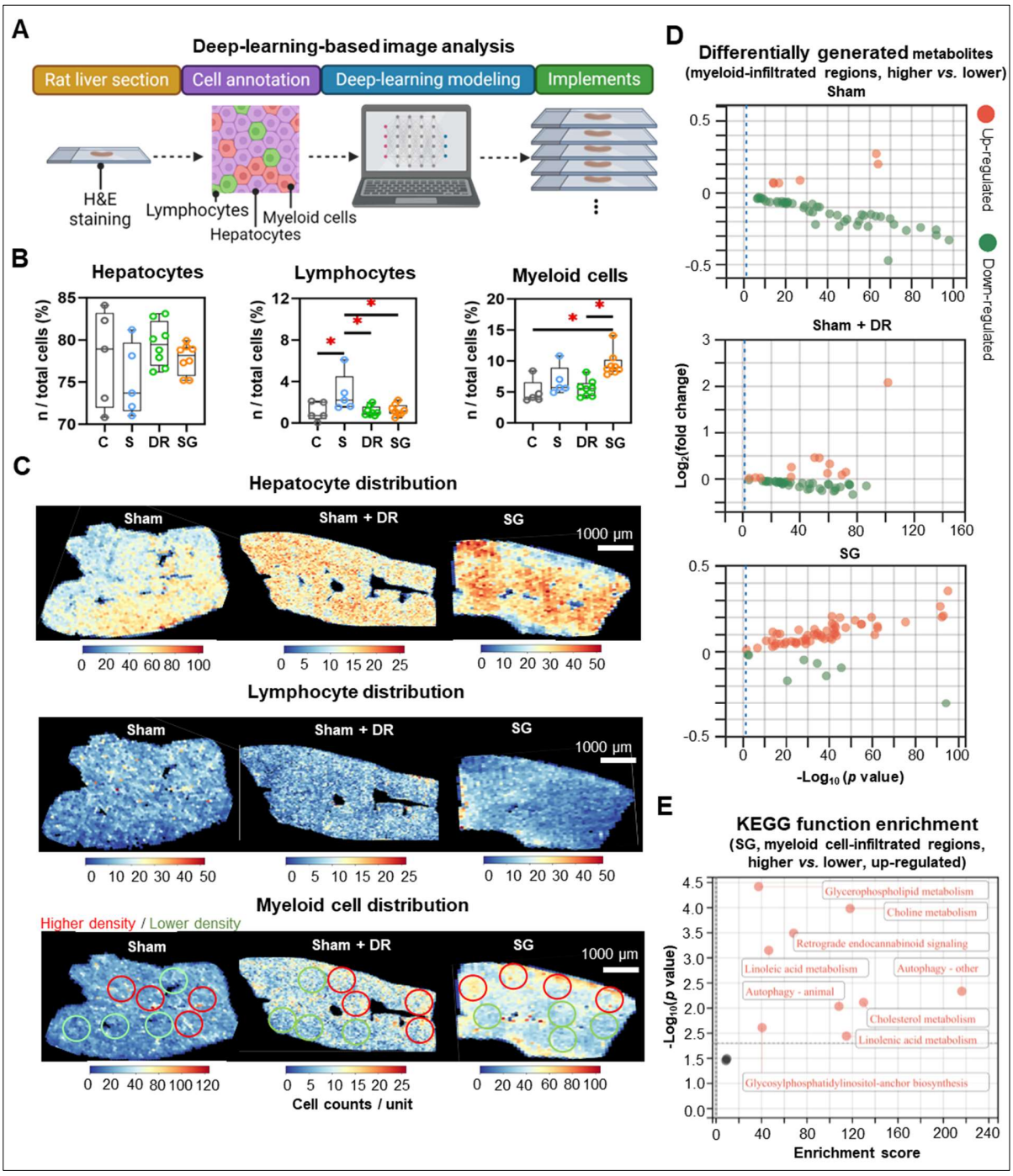
A
Deep-learning-based image analysis
Rat liver section
Cell annotation
Deep-learning modeling
Implements
H&E staining
Lymphocytes
Hepatocytes
Myeloid cells
B
Hepatocytes
Lymphocytes
Myeloid cells
n / total cells (%)
C S DR SG
C
Hepatocyte distribution
Sham
Sham + DR
SG
1000 μm
Lymphocyte distribution
Myeloid cell distribution
Higher density / Lower density
Cell counts / unit
D
Differentially generated metabolites
(myeloid-infiltrated regions, higher vs. lower)
Sham
Sham + DR
SG
Up-regulated
Down-regulated
Log2(fold change)
-Log10 (p value)
E
KEGG function enrichment
(SG, myeloid cell-infiltrated regions, higher vs. lower, up-regulated)
Glycerophospholipid metabolism
Choline metabolism
Retrograde endocannabinoid signaling
Linoleic acid metabolism
Autophagy - other
Autophagy - animal
Cholesterol metabolism
Linolenic acid metabolism
Glycosylphosphatidylinositol-anchor biosynthesis
-Log10(p value)
Enrichment score

852

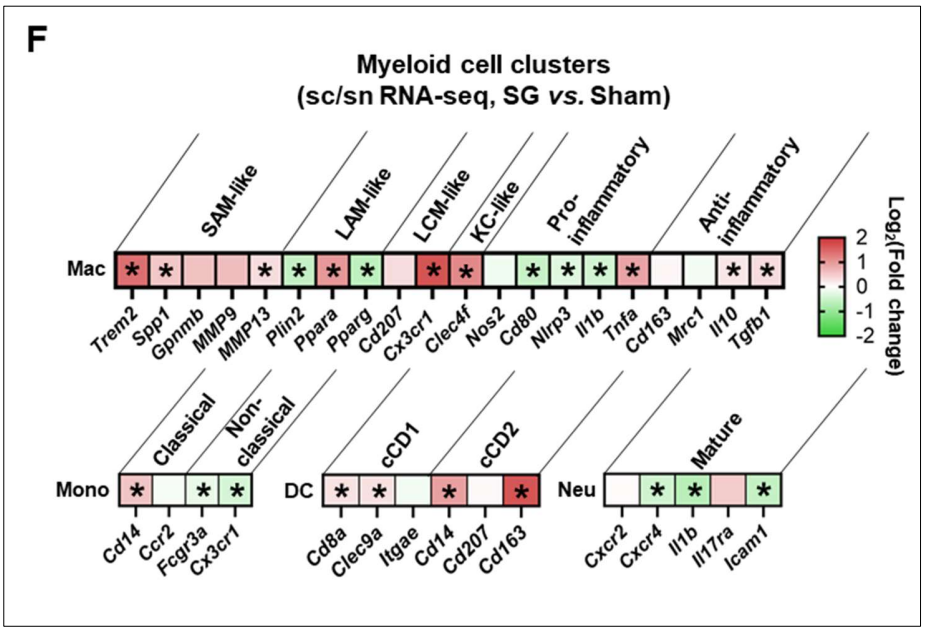

Figure 7. Sleeve gastrectomy facilitates lipid metabolism and phenotypic alterations in myeloid cells. (A) The technical scheme of the deep-learning-based image analysis. The deep-learning approach assessed (B) proportions of hepatocytes, lymphocytes and myeloid cells in total liver cells per tissue section and (G) spatial distribution in representative liver samples. Regions with higher (red circles) and lower (green circles) myeloid cell densities were selected (D) Differentially generated metabolites were illustrated (higher myeloid cell infiltrated regions vs. lower myeloid cell infiltrated regions) in Sham, Sham + DR and SG groups. (E) Function enrichment of upregulated differentially generated metabolites (higher myeloid cell infiltrated regions vs. lower myeloid cell infiltrated regions) in the liver sample of SG group was analyzed based on the KEGG database. (F) The expression of phenotype-associated markers in myeloid cell clusters were illustrated based on sc/sn RNA-seq data (SG vs. Sham). Abbreviations: C: control; Sham/S: sham surgery; DR: dietary restriction; SG: sleeve gastrectomy; KEGG: Kyoto encyclopedia of genes and genomes. sc/sn: single-cell/single-nuclei; Mono: monocytes; Mac: macrophages; DC: dendritic cells; Neu: neutrophils; SAM: scar-associated macrophage; LAM: lipid-associated macrophage; LCM: liver capsular macrophage; KC: Kupffer cell; cDC: conventional DC. The unpaired t-test and one-way ANOVA test were performed. '*' represents '$p < 0.05$' and statistical significance.

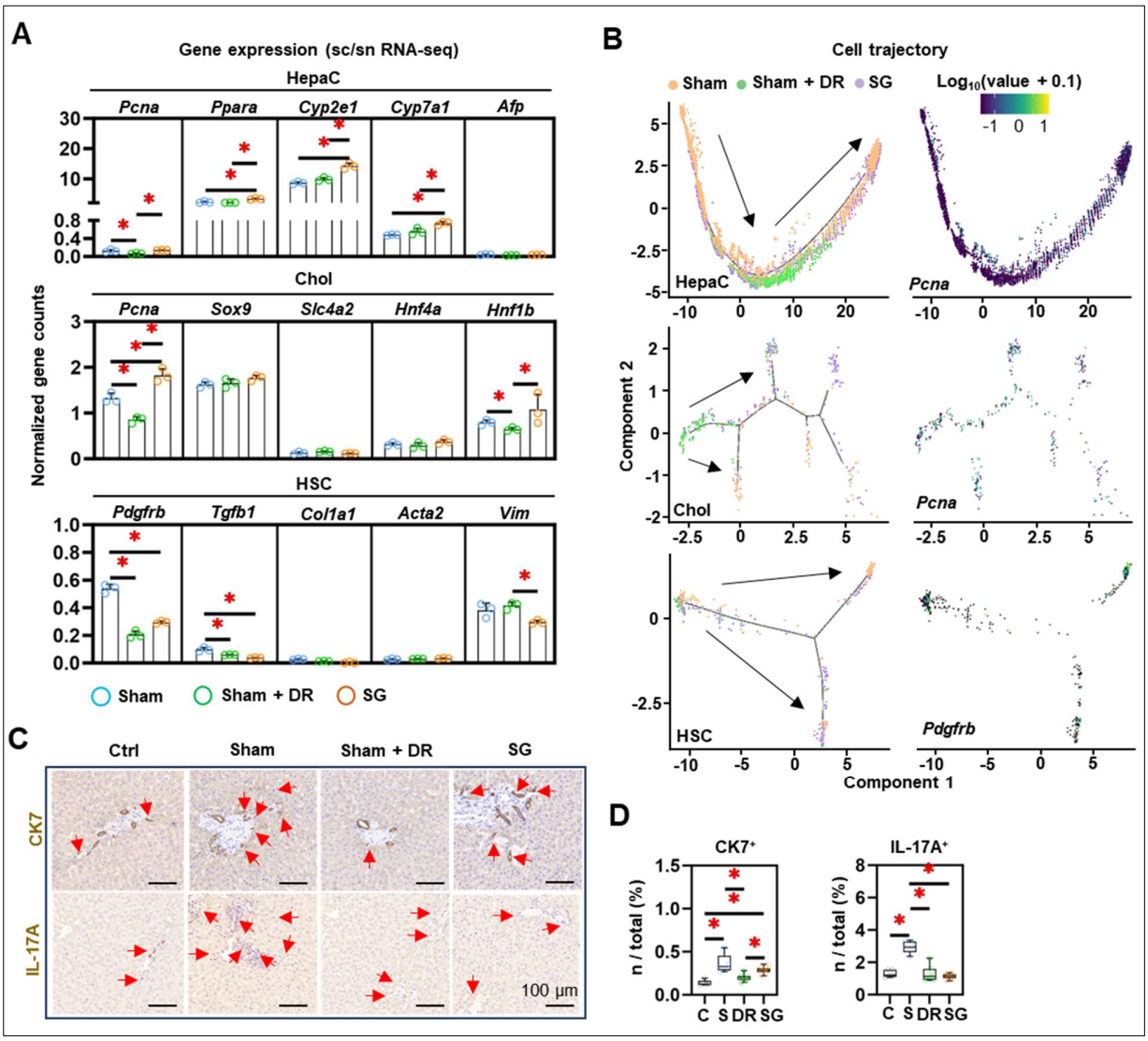

Figure 8. Dietary restriction and sleeve gastrectomy alter the cellular differentiation of hepatocytes, cholangiocytes and hepatic stellate cells. (A) Cellular characteristic markers of HepaC (Pcna, Ppara, Cyp2e1, Cyp7a1 and Afp), Chol (Pcna, Sox9, Slc4a2, Hnf4a and Hnf1b) and HSC (Pdgfrb, Tgfb1, Col1a1, Acta2 and Vim) were displayed. (B) Cell trajectories of HepaC, Chol and HSC together with Cyp2e1 expression in HepaC, Pcna expression in Chol, and Pdgfrb expression in HSC. CK7- and IL-17A- expressing cells were (C) illustrated in situ and (D) quantified from total rat liver cells. Abbreviations: C: control; Sham/S: sham surgery; DR: dietary restriction; SG: sleeve gastrectomy; HepaC: hepatocyte; Chol: cholangiocyte; HSC: hepatic stellate cell; KEGG: Kyoto encyclopedia of genes and genomes. The one-way ANOVA test was performed. '*' represents '$p < 0.05$' and statistical significance.

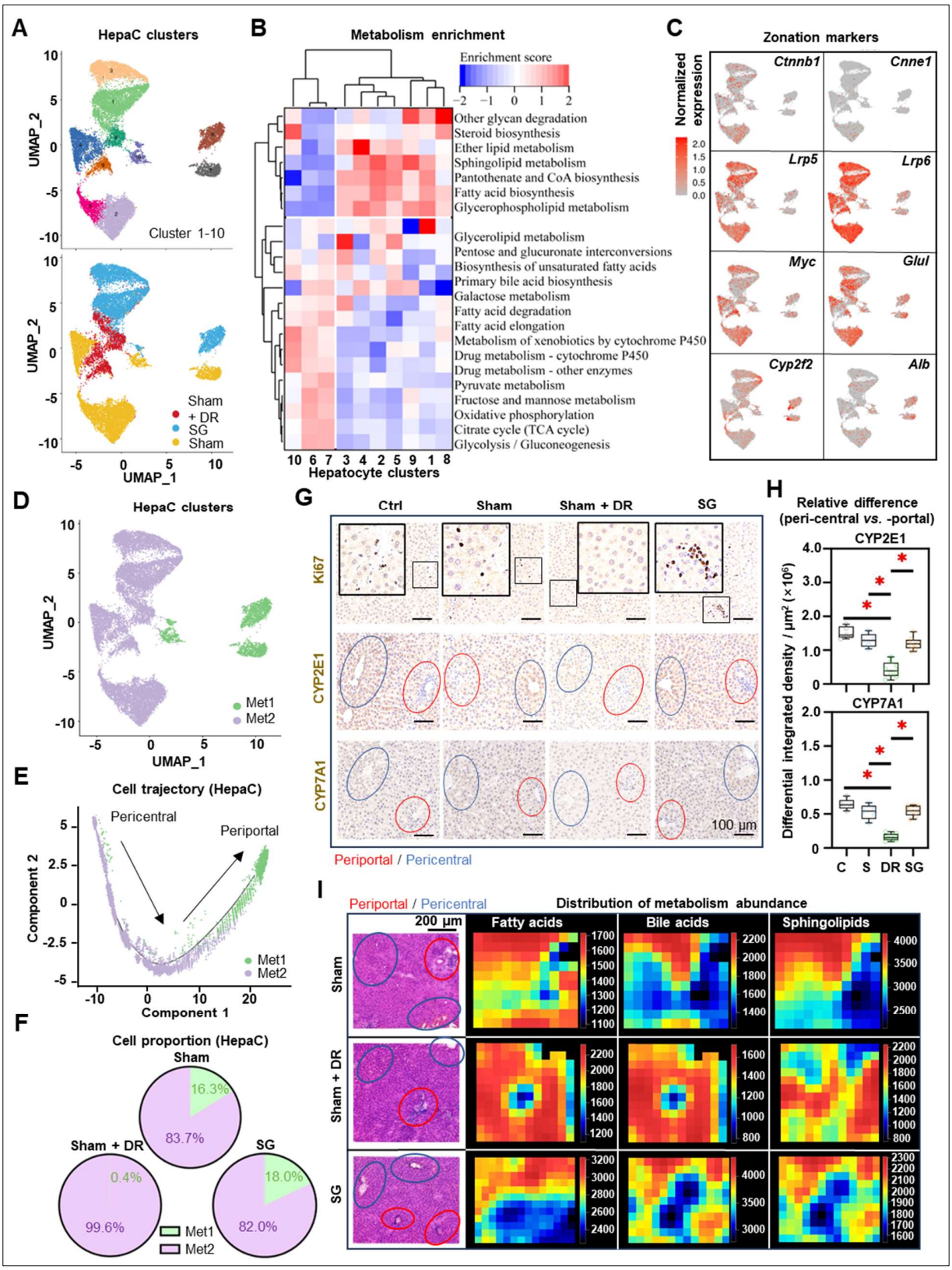
A
HepaC clusters
UMAP_2
UMAP_1
Cluster 1-10
Sham
+ DR
SG
Sham
B
Metabolism enrichment
Enrichment score
Other glycan degradation
Steroid biosynthesis
Ether lipid metabolism
Sphingolipid metabolism
Pantothenate and CoA biosynthesis
Fatty acid biosynthesis
Glycerophospholipid metabolism
Glycerolipid metabolism
Pentose and glucuronate interconversions
Biosynthesis of unsaturated fatty acids
Primary bile acid biosynthesis
Galactose metabolism
Fatty acid degradation
Fatty acid elongation
Metabolism of xenobiotics by cytochrome P450
Drug metabolism - cytochrome P450
Drug metabolism - other enzymes
Pyruvate metabolism
Fructose and mannose metabolism
Oxidative phosphorylation
Citrate cycle (TCA cycle)
Glycolysis / Gluconeogenesis
Hepatocyte clusters
C
Zonation markers
Normalized expression
Ctnnb1
Cnne1
Lrp5
Lrp6
Myc
Glul
Cyp2f2
Alb
D
HepaC clusters
Met1
Met2
E
Cell trajectory (HepaC)
Pericentral
Periportal
Component 1
Component 2
F
Cell proportion (HepaC)
Sham
16.3%
83.7%
Sham + DR
0.4%
99.6%
SG
18.0%
82.0%
Met1
Met2
G
Ctrl
Sham
Sham + DR
SG
Ki67
CYP2E1
CYP7A1
100 μm
Periportal / Pericentral
H
Relative difference
(peri-central vs. -portal)
CYP2E1
CYP7A1
Differential integrated density / μm² (×10⁶)
C
S
DR
SG
I
Periportal / Pericentral
Distribution of metabolism abundance
200 μm
Fatty acids
Bile acids
Sphingolipids
Sham
Sham + DR
SG

886

887 **Figure 9. Dietary restriction compromises zonation characteristics of periportal**
888 **hepatocytes.** (A) Subclusters of rat hepatocytes from Sham, Sham + DR and SG
889 illustrated in UMAPs. (B) Metabolism enrichment on each hepatocyte subcluster is
890 displayed in a matrix. (C) Gene expression of Ctnnb1, Cnne1, Lrp5, Lrp6, Myc, Glul,
891 Cyp2f2 and Cyp7a1 illustrated in rat hepatocytes. (D) Metabolism group-1 and -2 in rat
892 hepatocytes. (E) Metabolism group-1 and -2 in the cell trajectory of rat hepatocytes. (F)
893 Proportions of metabolism group-1 and -2 in rat hepatocytes of Sham, Sham + DR and
894 SG groups. (G) Protein levels of Ki67, CYP2E1 and CYP7E1 illustrated in rat liver tissue
895 (each view contains one or more portal and central areas) of Sham, Sham + DR and SG
896 groups. (H) Relative differences of CYP2E1 and CYP7E1 levels between peri-central and
897 -portal regions in each rat liver tissue of Sham, Sham + DR and SG groups. (I) Spatial
898 distribution of fatty acid, bile acid and sphingolipid metabolites. In H&E- and IHC-
899 characterized rat liver sample sections, periportal regions were outlined in red circles and
900 pericentral regions were outlined in blue circles. Abbreviations: Sham: sham surgery;
901 DR: dietary restriction; SG: sleeve gastrectomy; HepaC: hepatocyte; Met: metabolism;
902 CYP: cytochrome. H&E: hematoxylin and eosin. '*' represents '$p < 0.05$' and statistical
903 significance.

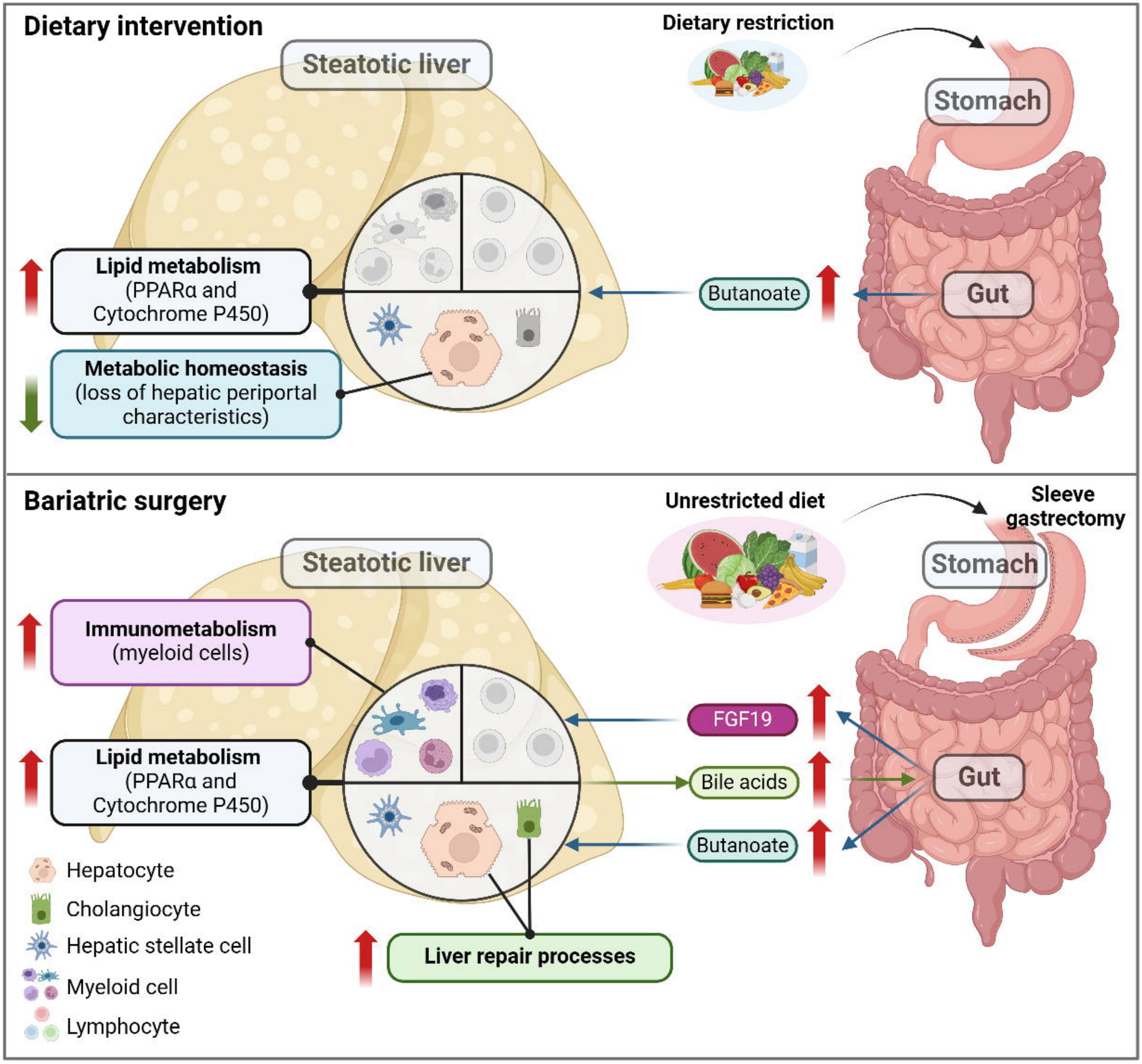
Dietary intervention
Dietary restriction
Steatotic liver
Stomach
Lipid metabolism
(PPARα and
Cytochrome P450)
Butanoate
Gut
Metabolic homeostasis
(loss of hepatic periportal
characteristics)
Bariatric surgery
Unrestricted diet
Sleeve
gastrectomy
Steatotic liver
Stomach
Immunometabolism
(myeloid cells)
FGF19
Lipid metabolism
(PPARα and
Cytochrome P450)
Bile acids
Gut
Butanoate
Hepatocyte
Cholangiocyte
Hepatic stellate cell
Myeloid cell
Lymphocyte
Liver repair processes